Quaternary Science Reviews 369 (2025) 109576

Contents lists available at ScienceDirect

Quaternary Science Reviews

journal homepage: www.elsevier.com/locate/quascirev

Millennial-scale climatic variability and fire regimes and their impacts on vegetation in Gran Canaria since since 28 cal ka BP

Pilar Martin-Ramos [a,*], Alvaro Castilla-Beltrán [a,b,c,**], Nina Davtian [d,e], José María Fernández-Palacios [a], Enrique Fernández-Palacios [c,f], Agustín Naranjo-Cigala [g], Sandra Nogué [h,i], Joan Villanueva [d], Janet M. Wilmshurst [j], Lea de Nascimento [a]

[a] Island Ecology and Biogeography Group, Universidad de La Laguna (ULL), San Cristóbal de La Laguna, Spain
[b] Disaster Risk Reduction and Resilient Cities Group, Universidad de La Laguna (ULL), San Cristóbal de La Laguna, Spain
[c] Archaeological Micromorphology and Biomarkers Laboratory (AMBI Lab), Instituto Universitario de Bio-Orgánica Antonio González, Universidad de La Laguna (ULL), San Cristóbal de La Laguna, Spain
[d] Institut de Ciència i Tecnologia Ambientals (ICTA-UAB), Universitat Autònoma de Barcelona, Bellaterra, Spain
[e] Aix Marseille Univ, CNRS, IRD, INRAE, CEREGE, Aix-en-Provence, France
[f] Institute of Prehistoric and Protohistoric Archaeology, Kiel University (CAU), Kiel, Germany
[g] Department of Geography, Universidad de Las Palmas de Gran Canaria (ULPGC), Las Palmas de Gran Canaria, Spain
[h] Departament de Biologia Vegetal, Biologia Animal i d'Ecologia (BABVE), Universitat Autònoma de Barcelona, Belaterra, Spain
[i] CREAF, Bellaterra, Spain
[j] Long-Term Ecology Laboratory, Manaaki Whenua – Landcare Research, Lincoln, New Zealand

ARTICLE INFO

Handling editor: Patrick Rioual

Keywords:
Canary Islands
CharAnalysis
Charcoal analysis
Climate reconstruction
Fire regime
Island vegetation
Macaronesia
Palaeoecology
Pollen climate model

ABSTRACT

The influence of climate change and fire regimes on vegetation in the Canary Islands at the millennial scale remains largely unknown. This study presents the longest continuous palaeoecological record from the archipelago, spanning the last 28,000 years from Vega de Arucas in Gran Canaria. Using a multiproxy approach, we analysed charcoal particles for fire frequency reconstruction, fossil pollen and non-pollen palynomorphs (NPPs) for vegetation change, sedimentology for changes in material deposited, branched glycerol dialkyl glycerol tetraethers (brGDGTs) for air temperature, and pollen climate modelling for temperature, precipitation, and relative humidity estimates. We document different changes in vegetation and fire regimes linked to regional and global climatic transitions. Before the Last Glacial Maximum (LGM), pollen and charcoal data indicate local presence of a laurel forest taxa (e.g., *Morella faya*) at low elevations (c. 200–300 m above sea level), subjected to infrequent fires, suggesting wetter conditions and cooler temperatures. During the LGM, the laurel forest was replaced by a dry pine forest, indicative of lower than previous temperatures and reduced water availability. This transition from laurel to pine forest coincides with an increase in fire frequency. During the last deglaciation (Bølling-Allerød and Younger Dryas), a rapid shift occurred from pine forest to thermophilous woodland (e.g., *Juniperus* sp., *Phoenix canariensis*), reflecting warmer conditions with continued climate oscillations and more frequent fire activity. Although pollen preservation was poor during the Holocene and hampers current understanding of vegetation changes throughout this period, charcoal records indicate frequent fires. While previous views have proposed that islands may have been buffered from climatic changes due to the regulating influence of the ocean, our study confirms a scenario of direct influence of global and regional climatic variations in local vegetation distribution and fire regimes. This has important implications for understanding vegetation resilience and landscape management in the face of future climatic changes.

* Corresponding author.
** Corresponding author. Island Ecology and Biogeography Group, University of La Laguna, Spain.
E-mail addresses: mariadelpilarmartin@gmail.com (P. Martin-Ramos), acastilb@ull.edu.es (A. Castilla-Beltrán).

https://doi.org/10.1016/j.quascirev.2025.109576
Received 28 March 2025; Received in revised form 12 August 2025; Accepted 13 August 2025
Available online 6 October 2025

1. Introduction

Understanding the long-term dynamics of climate, disturbances, and biodiversity on islands not only helps us comprehend their natural history but also allows us to forecast their responses to global change (Nogué et al., 2017). Future climate change predictions suggest islands will face warmer temperatures, shifts in rainfall patterns caused by ocean current changes, and variations in cloud cover (Sperling et al., 2004; Harter et al., 2015). These shifts are expected to severely impact island ecosystems, as their vulnerability is heightened by the low levels of functional redundancy of the insular biota (Gilman et al., 2010; Harter et al., 2015). The predictions result in a dual outcome: islands with low topographic complexity will experience heightened extinction rates, whereas those with more complex topography will serve as climate refuges (Harter et al., 2015). Furthermore, climate change is increasingly triggering extreme climatic events; however, the impact of these disturbances on oceanic islands remains poorly understood due to a lack of long-term observational records (Jansen et al., 2007). Globally, islands generally exhibit cooler, more humid, and less seasonally variable conditions compared to mainland areas at similar latitudes, primarily due to their elevation and oceanic surroundings (Weigelt et al., 2013). This oceanic influence has traditionally led island biogeographers to view islands as relatively stable systems, buffered by the ocean (Whittaker and Fernández-Palacios, 2007; Whittaker et al., 2023). However, early debates in this field highlighted the impact of climate changes (e.g., Pleistocene glaciations) on the rate of island endemism through, for example, shifts in island area, isolation and elevation (Fernández-Palacios et al., 2016; Weigelt et al., 2016; Norder et al., 2019; Whittaker et al., 2023). Furthermore, recent analyses of long-term multi-proxy sediment data are revealing evidence of islands' lack of stability in relation to climate and disturbance (Birks and Birks, 2006; Ljung and Björck, 2007; Jansen et al., 2007; Castilla-Beltrán et al., 2023). Long-term studies are essential for understanding island natural variability, providing a comprehensive temporal perspective that enables researchers to contextualise recent ecological changes with previous natural dynamics (Willis and Birks, 2006). In terms of climate reconstruction, terrestrial records from islands provide advantages over mid-ocean marine cores. They can provide much higher temporal and spatial resolution regarding terrestrial biodiversity responses to change and avoid radiocarbon dating complications associated with the marine reservoir effect (Björck et al., 2006; Ljung and Björck, 2007). For example, palaeoecological studies in Mauritius (Indian Ocean) reveal hydrological dynamics related to ENSO, showing shifts between wetland and lake conditions influenced by sea level rise and precipitation changes (de Boer et al., 2013). Similar studies in the Azores (Atlantic Ocean) have shown precipitation changes linked to shifts in the North Atlantic thermohaline circulation (Björck et al., 2006; Richter et al., 2022).

Due to their isolation, small size, elevational and climatic gradients, oceanic islands provide valuable settings for understanding natural environments (Whittaker et al., 2023). Moreover, islands host high levels of endemicity, which in turn are highly threatened, and thus some are considered biodiversity hotspots on the planet (Nogué et al., 2017; Fernández-Palacios et al., 2021). On the other hand, oceanic islands are among the most recently colonised areas on Earth, often within the last few millennia or centuries (Nogué et al., 2021, 2022). This relatively recent colonisation allows for the examination of natural fire regimes related to climate for comparison with later human-driven fires (Nogué et al., 2024). In Hawaii (Pacific Ocean), tropical forests have shown remarkable stability and resilience in the face of wildfires and drought (Crausbay et al., 2014). Similarly, fires in Corsica (Mediterranean Sea) function as natural landscape engineers (Leys et al., 2014; Lestienne et al., 2019). By contrast, in New Zealand where natural fires were infrequent during the Holocene, recent human arrival dramatically increased fire frequency and extent, reducing forest cover from 85–90 % to 25 % of the land area since the 13th century (McWethy et al., 2010, 2014; Perry et al., 2014).

The Canary Islands are located near the northwestern coast of the Sahara Desert, harboring a unique biodiversity with over 17,800 terrestrial species, of which a large proportion are endemic (Banco de Datos de Biodiversidad de Canarias, 2024). The earliest human presence in the Canary Islands dates c. 2000 cal a BP, although this timing varies between islands (Santana et al., 2024). Palaeoecological studies conducted in Tenerife (de Nascimento et al., 2009), Gran Canaria (de Nascimento et al., 2016; Ravazzi et al., 2021), and La Gomera (Nogué et al., 2013) have demonstrated shifts in vegetation and fire occurrences during the Holocene. These shifts were linked to human colonisation in Tenerife and Gran Canaria, and to decreased humidity/precipitation in La Gomera. Ecological succession studies in the Canary Island laurel forests suggest that these communities are highly susceptible to fire, and their fundamental characteristics—such as structure, composition, and microclimate—showing significant alterations that can still be detected up to 50 years later (Bello-Rodríguez et al., 2018). By contrast, in the Canary Island pine forest, *Pinus canariensis* exhibits morphophysiological adaptations that enhance its fire resistance (Climent et al., 2004; Ne'eman and Arianoutsou, 2021) while the fire resistance of other accompanying species remains less well-understood (Garzón-Machado et al., 2012). Ecological monitoring studies on structure, sexual regeneration, species richness, and composition of pine forests suggest complete recovery after fire (Otto et al., 2010; Arévalo et al., 2014; Méndez et al., 2015). Moreover, the vulnerability and resilience of key zonal ecosystems to climate change have become a central focus of research, particularly in mid and high-elevation habitats such as the laurel forest (Sperling et al., 2004; García-López et al., 2022), the pine forest (Bello-Rodríguez et al., 2019; Navarro-Cerrillo et al., 2024), and the summit scrub (Olano et al., 2017; Martín-Esquivel et al., 2020). These studies have provided long-term insights into the complex interplay between climate, vegetation, and fire regimes in the Canarian archipelago during the Holocene. However, several knowledge gaps remain around longer-term fire frequency, vegetation and climate change that inhibit our ability to predict resilience to future global change.

1) *Understanding the influence of past climate changes on biodiversity*: Despite regional studies spanning the Late Pleistocene that have explored broader climatic influences on marine/coastal biodiversity (e.g., Yanes et al., 2011), local terrestrial evidence of climate shifts is scarce. Additionally, most of the available information from this period is from studies on the eastern islands (Lanzarote and Fuerteventura) (Damnati et al., 1996; Coello et al., 1999; Lomoschitz et al., 2008). The knowledge of past vegetation dynamics is limited to the Holocene due to the scarcity of permanent lakes (Anderson et al., 2009). The combination of fossil and subfossil data with recently developed geochemical methods on available long-term records could be used to infer past climate conditions during a more climatically variable epoch such as the Pleistocene (Jansen et al., 2007).
2) *Fire regime reconstruction*: Although previous palaeoecological studies in the Canary Islands have examined charcoal sequences, these studies have not employed robust or standardised statistical models. Implementing new statistical analyses could improve the identification of historical fires and the quantification of long-term natural variations, establishing their relationships with vegetation and climate dynamics (Conedera et al., 2009).
3) *Pre-human lowland vegetation dynamics*: The dynamics and composition of past vegetation in the lowlands of the Canary Islands remain poorly understood, as previous palaeoecological studies have been on midland and highland areas. This is due to the inherent challenges of working on drier conditions prevailing at low elevations (Brunelle et al., 2018), as well as the alteration of potential sites due to modern intensification of human activities on coastal areas.

In this paper, we address these knowledge gaps by assessing the

interaction between fire frequency, vegetation, and climate changes. We focus on a 28,000-year record from a lowland area (226 m a.s.l., above sea level) in Gran Canaria, marking it as the first terrestrial late Pleistocene palaeoecological record from the Canary Islands. Using a multi-proxy approach, including charcoal, pollen and non-pollen palynomorph (NPP) analysis, sedimentology, and pollen climate modelling, complemented by an organic geochemical proxy based on bacterial membrane lipids (branched glycerol dialkyl glycerol tetraethers, brGDGTs) for temperature reconstructions, we examine the role of regional climate changes on the fire regimes and ecology of a lowland valley. By studying environmental changes with rigorous statistical methods, we develop a more robust understanding of how ecosystems adapted to past climate changes. Finally, this research provides the first approximation to long-term natural (pre-human) fire regimes,

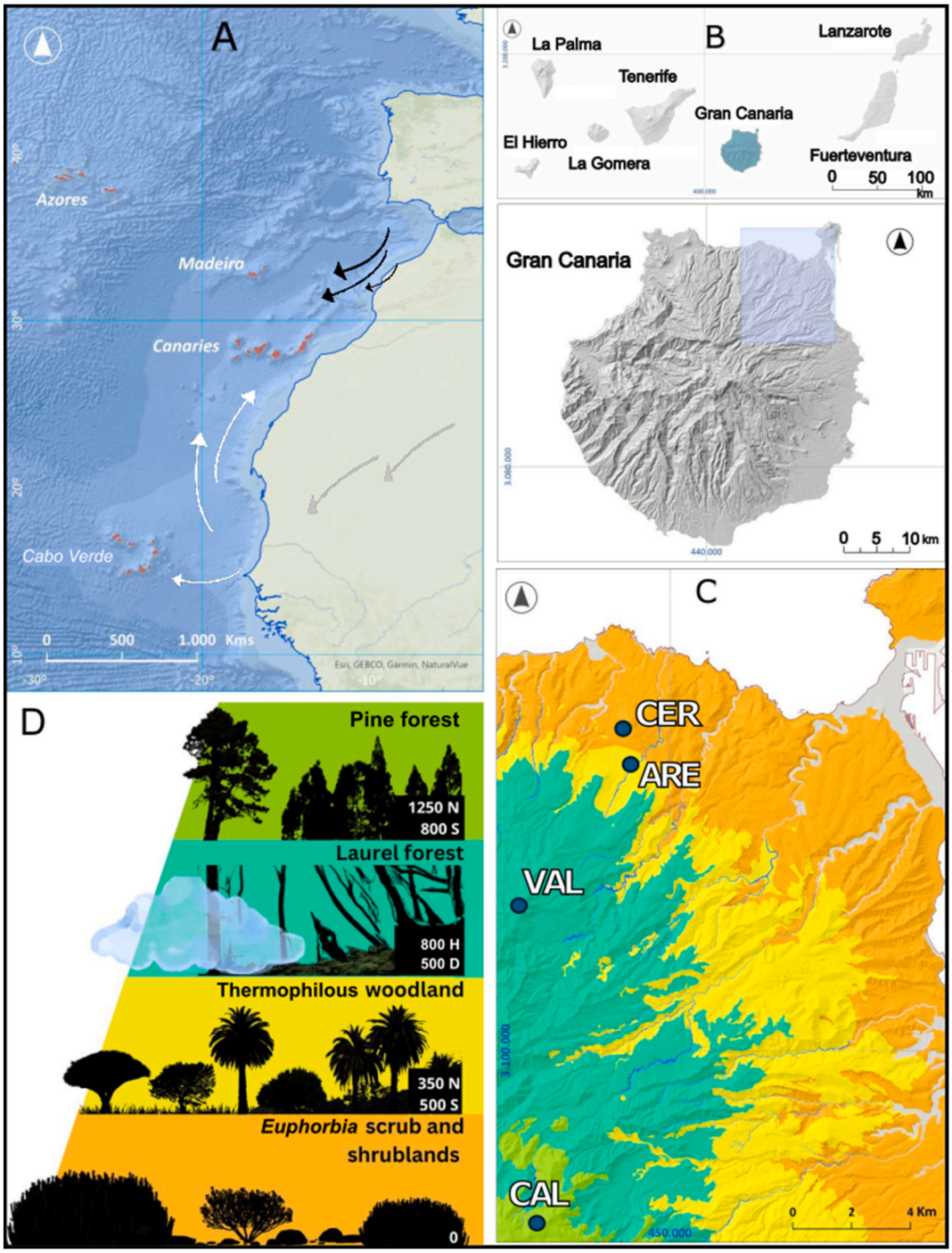

Fig. 1. Map of the study area. A. General view of Macaronesia, based on Natural Earth public domain map dataset. Black arrows represent trade winds; grey arrows represent Harmattan winds; and white arrows represent the Saharan Air Layer. B. General view of the Canary Archipelago, adapted from a topographic map (GRAFCAN, 2004). Topographic map of the island of Gran Canaria, based on GRAFCAN (2004). C. Location of the sedimentary records of Gran Canaria, marked as blue dots, over the potential vegetation map, plotted from the Canary Islands vegetation map (del Arco et al., 2006): CAL (La Calderilla), VAL (Laguna de Valleseco), ARE (Vega de Arucas), and the archaeological record of La Cerera (CER). D. Main vegetation types in Gran Canaria with minimum elevational range N (North); S (South); D (dry laurel forest), H (humid laurel forest). (For interpretation of the references to colour in this figure legend, the reader is referred to the Web version of this article.)

helping to inform the debate on prescribed burning and fire suppression in forest management (Arévalo et al., 2001; Garzón-Machado et al., 2012; Arévalo and Naranjo-Cigala, 2018; Arévalo et al., 2023). This approach is crucial for forecasting future ecological responses in the context of ongoing climate change and anthropogenic impacts.

2. Material and methods

2.1. Study area

2.1.1. Gran Canaria

The Canarian archipelago comprises seven main islands that cover an area of 7447 km^2. It is located 95 km off the Saharan coast, approximately 27–29 °N latitude and 23–18 °W. Gran Canaria, the third largest and highest island in the archipelago, spans an area of 1560 km^2. Its highest elevation is at Pico de las Nieves in the island center, reaching 1950 m a.s.l. As a result of hotspot volcanism, Gran Canaria is characterised by rugged terrain with high volcanoes, steep cliffs, caves, deep gorges and ravines. Geologically, the island consists of the volcanically active "Neocanaria" in the northeast, rejuvenated in the Pliocene and Pleistocene, and the long-dormant "Paleocanaria" in the southwest, dominated by Miocene substrates (Schmincke and Sumita, 2012). Its climate is conditioned by the cold Oceanic Canary Current and the dominant northeastern trade winds (Fig. 1). While the Atlantic storms associated with autumn and winter bring rain to the islands and snow to the peaks of the highest mountains, the archipelago also experiences occasional dry winds from the Sahara (Marzol Jaén and Máyer Suárez, 2012). Temperature and rainfall in the Canary Islands generate an altitudinal gradient where the influence of the NE trade winds forms a sea of clouds between 400–600 and 1200–1500 m a.s.l., and brings humidity to windward facades through horizontal rain. The vegetation is organised in distinct altitudinal belts: coastal *Euphorbia* scrub and shrublands, followed by mid-elevation thermophilous woodland, then laurel forests located at the windward slopes of the island, and finally Canary pine forest at higher elevation (Fig. 1) (del Arco and Rodríguez Delgado, 2018).

To facilitate discussion of past bioclimatic stages in the archipelago, we provide a brief description of the four main vegetation types, and their associated climatic variables based on del Arco Aguilar and Rodríguez Delgado (2018).

1. *Euphorbia scrub and shrublands* are succulent communities typically found in the coastal regions of the islands, reaching coastal cliffs in the north and extending up to 800 m a.s.l. in the south. These areas, characterised by rocky and scarcely developed soils, endure an arid to semi-arid climate with minimal rainfall ranging between 50 and 300 mm annually. The temperatures are high, with an annual average above 19 °C, and there is significant sun exposure. This environment supports various *Euphorbia* species, some of which are known as dendroid spurges (i.e. *Euphorbia balsamifera*), which dominates the “tabaibal dulce” (sweet spurge scrub), while others exhibit a candelabra-like form typical of cactiform spurges (i.e. *Euphorbia canariensis*), which dominates the “cardonal” (cardón scrub).
2. *Thermophilous woodlands* occur in the midlands of the island, up to 500 m a.s.l. in the north and between 500 and 800 m a.s.l. in the east. The average annual temperature in these areas ranges from 15 to 19 °C, with rainfall between 250 and 400 mm. The vegetation consists of relatively open communities of *Juniperus turbinata* subsp. *canariensis*, *Olea cerasiformis*, *Pistacia atlantica*, and *P. lentiscus*. The structure of the woodland varies based on the dominant tree species: *P. atlantica* tends to populate valleys and foothills, whereas *O. cerasiformis* and *J. turbinata* subsp. *canariensis* are more adapted to drier conditions. The humid slopes and ravines also host a *Phoenix canariensis* palm community (Fernández-Palacios et al., 2024).
3. *Humid laurel forests* are found at an elevation between 800 and 1250 m a.s.l. in the windward slopes, in areas with an average annual temperature between 13 and 18 °C and annual rainfall ranging from 500 to 1200 mm. The presence of clouds plays a crucial role in their survival by maintaining the forest’s water balance and reducing evaporation, which is vital during the dry Mediterranean summers. The dominant tree species belong to the Lauraceae family, including *Laurus novocanariensis, Persea indica, P. barbujana*, and *Ocotea foetens*, along with representatives from other families such as *Heberdenia excelsa* (Primulaceae), *Ilex perado* subsp. *platyphylla* (Aquifoliaceae), *Picconia excelsa* (Oleaceae), and *Visnea mocanera* (Pentaphylacaceae) and among others. There is also a dry laurel forest, a thermophilic community that is drier and warmer than other types of laurel forest and forms under the fluctuating direct influence of the cloud bank, located between 500 and 800 m a.s.l. It includes drought-resistant species such as *Persea barbujana*, *Picconia excelsa*, and *Visnea mocanera*, as well as *Morella faya*. Additionally, the “fayal-brezal” is a substitutional shrubland of the laurel forest, primarily expanded due to human disturbance, consisting mainly of *Erica canariensis, Morella faya,* and *Ilex canariensis* (Fernández-Palacios et al., 2017).
4. *Canary pine forest* thrives above the cloud belt in the north and just above the thermophilous woodland in the south. It is found at an elevation between 1250 and 1950 m a.s.l. in the north between 800 and 1950 m a.s.l. in the south. However, these elevation limits can be exceeded because of the competitiveness of pine on salic substrates and recent lava flows. These areas have average annual temperatures ranging from 11 to 15 °C and receive approximately 450–600 mm of rainfall annually. Canary pine forest is characterised by the presence of *Pinus canariensis*, and a broad spectrum of conditions, from dry to humid.

2.1.2. Study site: Vega de Arucas

The Vega de Arucas, situated at an elevation of 226 m a.s.l. (Fig. 1), is a basin, 2 km in diameter, filled with sediment formed after the eruption of the Montaña de Arucas volcano 310,000 years ago (Lietz and Schmincke, 1975). The eruption blocked the original path of the Arucas and Travieso ravines, causing the accumulation of sediment in the basin. Once filled, the ravine created a new outlet towards Cardones village (Díaz Elías, 2014).

Although recent historical sources do not indicate the presence of permanent lakes in Gran Canaria, older historical evidence suggests the existence of some water bodies. Early records from the 16th century found in the "Libro de Memoria Antiguas" (page 93) and the "Libro 2° de Cuadrantes de Misas" (page 59) kept in the Parish Archive of San Juan Bautista de Arucas, contain several references to the "Laguna de Barreto" (Barreto Lake) (Caballero Mujica, 1974). Additionally, it has been hypothesised that multiple freshwater mires might have been present in this area during pre-conquest periods (Medina, 2004).

According to climatic records, this area currently receives annual rainfall of approximately 200 mm and has a mean annual temperature of 20 °C (Agencia Estatal de Meteorología, 2024). The potential vegetation of the Vega de Arucas has been described as a hygrophilous Canary Island palm tree community (del Arco et al., 2006). To the coast, it transitions into *Euphorbia canariensis* scrub, and to the summit, it transitions into a thermophilous woodland. Just a few kilometers further south, this thermophilous woodland gives way to a dry laurel forest (del Arco et al., 2006) (Fig. 1). The earliest evidence of human presence in the area comes from the La Cerera site, located approximately 1000 m from La Vega (Jiménez Medina, 1994). This site suggests an initial occupation around 1650 ± 40 cal a BP, or 1410 ± 30 cal a BP, with minimal anthropogenic impact. This was followed by a demographic expansion around the 7th century, likely associated with increased agricultural transformation of the landscape (Becerra Romero et al., 2009). Since the 15th century, the fertile soils of Vega de Arucas have been used for agriculture, starting with sugarcane cultivation (15th–16th centuries), followed by cereals and legumes for

self-consumption, viticulture (17th–19th centuries), and finally banana farming (Díaz Fernández, 1989).

2.2. Sample collection

In July 2017, a 4.62 m sedimentary sequence was retrieved from Vega de Arucas (ARE) without hitting rock bottom. Universal Transverse Mercator coordinates: Zone 28, 448602, 3109702, Elevation: 226 m a.s.l. The first 50 cm of the sedimentary sequence, dating from 1570 cal a BP to the present, contained a mix of materials including fragments of tiles, stones and metal pieces and were discarded due to anthropogenic mixing from agricultural activities.

Currently, the area has abandoned crops and a sugarcane plantation for rum production. The samples were collected in 60 cm sections using an automatic drilling machine, preserved in PVC tubes, and the 6 cm tips at the drill head were stored in zip-lock bags at 4 °C in the cold room of the Instituto Universitario de Enfermedades Tropicales y Salud Pública de Canarias, University of La Laguna. Subsequently, the sediment sections were opened for detailed sedimentological analysis and subsampling.

2.3. Radiocarbon dating

Radiocarbon dates from bulk sediment were obtained using Accelerator Mass Spectrometry (AMS) in two different laboratories (Chrono Centre at Queen's University Belfast and Beta Analytic) (Table 1). Attempts to date small charcoal fragments, seeds and several levels of bulk sediment were unsuccessful (see Table S1 and Supplementary text 1).

2.4. Laboratory analyses

2.4.1. Pollen, spores and microcharcoal (<150 μm) analyses

The core was sub-sampled every 10 cm depth (a total of 37 samples) to analyse pollen and non-pollen palynomorphs (NPPs). The preparation of pollen, spores, and charcoal followed Bennett and Willis (2001) protocol for fossil pollen analysis, including microfiltration to raise the concentration of microfossils per sample. To concentrate microfossils and make them visible and countable under a microscope, 1 cm^3 of sediment had to be processed through several physical and chemical processes. This involved removing all other organic and inorganic materials.

A *Lycopodium* spore tablet of known concentration was added to each sample (batch 10922211, 17,197 spores per tablet) serving as a marker to estimate the microfossil concentration in a known volume of sediment. The sediment was treated with sodium pyrophosphate to disaggregate clays. Treated samples were sieved using 150 μm meshes to isolate the fraction containing microcharcoal fragments and other macrofossils. The finer fraction was separated by gravity using sodium polytungstate with a relative density of 1.9 g/cm^3 and sieved through 10 μm filters to remove silts and clays. The separated fraction underwent acetolysis with a mixture of sulfuric acid and acetic anhydride to remove polysaccharides. Finally, the sample was stained with aqueous safranin, dehydrated with isopropanol, and mounted in silicone oil. Pollen grains, fern spores and NPPs were counted at ×400 magnification, reaching a sum of 300 pollen grains in samples with abundant pollen grains, and a sum of >100 in samples with poor preservation and low pollen concentration (with the exception of sample 320 cm, with 78 grains). We used the software Tilia (version 2.0.41) to plot the pollen diagram, and carried out stratigraphically constrained CONISS analysis (Grimm, 1993). Microcharcoal particles (<150 μm) were counted in pollen slides until a total sum of 200 elements (microcharcoal and *Lycopodium* spores) was reached (Finsinger and Tinner, 2005).

Table 1
Radiocarbon-dated bulk sediment samples of the ARE record, Gran Canaria. Dates calibrated using the rcarbon package (Crema and Bevan, 2021) calibration curve IntCal20, RStudio program. See Table S1 for extended version.

Depth (cm)	Laboratory code	Radiocarbon age ^{14}C and error (years BP)	Calibrated age range (with median) years BP (95.4 %)
60	UBA_41360	2074 ± 23	2114 (2034) 1988
148	Beta_690055	10500 ± 40	12670 (12548) 12638
160	Beta_682196	9650 ± 30	11186 (11083) 11068
267	Beta_682197	10760 ± 30	12754 (12735) 12713
325	Beta_690051	11870 ± 40	13794 (13702) 13605
398	Beta_690056	21680 ± 90	26233 (25932) 26166
450	UBA_41362	23246 ± 163	27746 (27497) 27261

2.4.2. Macrocharcoal quantification (>150 μm)

Macrocharcoal quantification was conducted at high-resolution, with continuous subsampling at 2 cm intervals, with each sample measuring 2 cm^3 and resulting in a total of 203 samples. The volume of each sample was measured using volumetric displacement in distilled water. Due to the high clay content of the samples, a pre-treatment with sodium pyrophosphate at 70 °C for 10 min was first applied, although this did not improve disaggregation. Consequently, the samples were processed by sieving through a 150 μm mesh and further disaggregated with water. Subsequently, samples were thoroughly rinsed with distilled water to remove any remaining impurities. Macrocharcoal particles were identified and counted under a microscope. Based on these counts, macrocharcoal concentrations were calculated per unit volume of sediment.

2.4.3. Glycerol dialkyl glycerol tetraether (GDGT) analysis

For GDGT (glycerol dialkyl glycerol tetraether) analysis, samples were taken at variable resolutions: every 20 cm for the first 150 cm (covering the Holocene) and every 10 cm in deeper sections representing the deglaciation and the Last Glacial Maximum (LGM), totaling 28 samples. The GDGT content was analysed at the Laboratory of Stable Isotope Analysis of the Institute of Environmental Science and Technology at Universitat Autònoma de Barcelona (ICTA-UAB).

Initial viability checks were performed on five samples per sediment sequence to confirm the presence of GDGTs. Following confirmation, the remaining samples were analysed with higher resolution in sections representing the deglaciation and LGM due to their climatic variability. Between 1.5 and 2.9 g of dry, homogenised sediment were used for lipid extraction with dichloromethane:methanol (9:1 v:v) at 100 °C, employing ICTA-UAB's pressurised liquid extraction technology (ASE-350 Dionex Thermo). Known quantities of internal standards were added before lipid extraction for GDGT quantification.

Organic extracts were separated into two fractions using column chromatography (silica gel columns): an apolar fraction containing compounds such as *n*-alkanes (hexane:dichloromethane 9:1 v:v), and a polar fraction (dichloromethane:methanol 1:1 v:v) containing GDGTs. The GDGT fraction was filtered through a 0.45 μm polytetrafluoroethylene filter and analysed using high-performance liquid chromatography (Agilent 1290 Infinity) coupled with atmospheric pressure chemical ionisation mass spectrometry (Agilent 6470 triple quadrupole mass spectrometer used in single quadrupole mode) following the method described in Hopmans et al. (2016). Individual GDGT compounds were identified based on their retention times and masses ($[M + H]^+$ ions with *m/z* 1302.3, 1300.3, 1298.3, 1296.3, and 1292.3 for isoprenoid GDGTs and $[M + H]^+$ ions with *m/z* 1050.0, 1048.0, 1046.0, 1036.0, 1034.0, 1032.0, 1022.0, 1020.0, and 1018.0 for branched GDGTs, brGDGTs) using the MassHunter software, with their peak areas compared to that of the internal standard ($[M + H]^+$ ion with *m/z* 1208.2) to determine GDGT concentrations in ng/g of sediment.

This protocol for GDGT analysis was validated in the frame of the latest inter-laboratory study (De Jonge et al., 2024a) which focused on brGDGTs. A single sediment sample from the continental slope off the Ebro River was analysed repeatedly to monitor instrumental drift. Multiple aliquots of a sediment sample from a lake in mainland Spain were processed and analysed independently to assess the repeatability of

the protocol.

2.4.4. Sedimentology (granulometry, XRF-LOI)

Granulometric analysis was conducted on 41 samples with an approximate resolution of 10 cm. We used a Malvern Mastersizer-Hydro located at the School of Geography and Environmental Science, University of Southampton, selecting soil analysis settings for non-spherical particles. We adjusted obscuration and averaged 20-s measurements if the standard deviation was below 5 %. Results are expressed as median grain size, fractions (Dx10, Dx15, Dx90) and percentages of clay, silt, and sand.

For sediment elemental composition analysis, we conducted 160-s measurements on 41 bulk samples using a mounted hand-held X-Ray Fluorescence (XRF) device (Niton XL3T GOLDD). The semi-quantitative results are reported as detected elements in percentages and presented as ratios for palaeoenvironmental interpretation (Croudace and Rothwell, 2015).

To estimate the organic matter content of the same 41 sediment samples, we ashed the dried material from the same sample with an oven set at 550 °C for 4 h. After cooling, we calculated the weight loss on ignition (LOI) using a high precision balance by weighing the samples before and after (Heiri et al., 2001). All results were plotted using Tilia and Sigmaplot softwares.

2.5. Data analysis

2.5.1. Age-depth model and zonation

We developed a Bayesian age depth model with the seven successful bulk sediment radiocarbon dates (Table 1) using rbacon package, (RStudio version 1.1.456), dividing the record in 15 cm increments (29 sections) to account for rapid sedimentation changes reflected in the middle section of the record (Blaauw and Christen, 2013). Radiocarbon ages were calibrated with the IntCal20 curve (Reimer et al., 2020). The results are presented as calibrated thousands of years Before Present (cal ka BP) (where "present" is defined as the year 1950 CE) (Fig. S1 and Supplementary text 1).

As lack of pollen preservation in a substantial part of the record limits the division in pollen zones (see discussion sections 4.3 and 4.4), we used the results of the age-depth model to divide the record into chronological zones (ARE-1 to ARE-6) for result description and discussion based on six Northern Hemisphere climatic periods: pre-LGM: pre-Last Glacial Maximum (30–26 cal ka BP), LGM: Last Glacial Maximum (c. 26–14.5 cal ka BP), B/A: Bølling-Allerød (14.5–12.9 cal ka BP), YD: Younger Dryas (12.9–11.7 cal ka BP), AHP: African Humid Period (11.7–5 cal ka BP), M-LH: Middle and Late Holocene (5 cal ka BP –present).

2.5.2. Pollen-based climate model

Quantitative precipitation, temperature, and humidity records were obtained from pollen data using the CREST (Climate REconstruction SofTware) method as described by Chevalier et al. (2014). CREST utilises modern plant distributions and current climate data to define Probability Density Functions (PDFs), minimizing distortion from extreme values compared to conventional methods like Mutual Climate Range. This method also incorporates information from species abundance. Specific climatic envelopes for each taxon were determined using a custom database derived from Luque Söllheim et al. (2024) and Banco de Datos de Biodiversidad de Canarias (2024)to improve the resolution. From Luque Söllheim et al. (2024), climatic variables were extracted, while the species distribution data were obtained from the Banco de Datos de Biodiversidad de Canarias (2024). Climatic conditions for each taxon's presence coordinates were extracted and used to apply the CREST method via the crestrpackage.

CREST employs a two-step process to define probabilistic links between climate and pollen taxa. First, simple parametric PDFs are fitted for each plant species composing the pollen taxa, then averaged to estimate the collective response. Second, climate reconstructions are estimated by multiplying these PDFs with weights derived from observed abundances. To mitigate taphonomic biases and differential production rates among taxa, taxon percentages were normalised against the average observed percentages in the complete fossil sequence (Chevalier et al., 2014, 2020). The resulting posterior distribution from the multiplication of taxon PDFs provides the best estimate of climatic parameters and their uncertainties. It is important to note that such modelling assumptions carry important uncertainties and require further calibration and study. Given model uncertainties and limitations, we interpret the results cautiously alongside our other palaeoecological indicators.

2.5.3. CharAnalysis

Data analysis followed the methodological framework proposed by Higuera et al. (2010), utilizing a statistical peak detection method for reconstructing local fire histories from charcoal records in sediments. Model construction was executed using RStudio and the tapas package (Finsinger and Bonnici, 2022). The core exhibits sharp variations in sedimentation rates, which could potentially mask fire events (Higuera et al., 2010). To distinguish areas with good temporal resolution from those with very rapid sedimentation rates, the sequence was analysed in the following intervals, based on sedimentation rate changes: 1392–10, 049 cal a BP, 10,912–13,535 cal a BP, 13,569–25,664 cal a BP, and 25, 848–27,852 cal a BP.

The first step in the peak detection model involved interpolating charcoal concentrations at a constant temporal resolution to avoid biases in sediment segments, forming a series (C). Due to variable sedimentation rates in the ARE sequence (15–167 years/cm), interpolation was divided into four zones based on sedimentation rates to balance resolution. Next, series C underwent detrending, modelling slow changes in the mean (background component, Cback) using curve-fitting algorithms. Three smoothing methods were compared: robust loess, robust lowess, and moving median. Robust lowess was selected for its precise fit. Cpeak values required a threshold to separate fire-related variability from independent variability. We applied a local threshold of 0.95 using a Gaussian mixture model for precision, following Higuera's (2009) recommendations. To eliminate statistically insignificant charcoal counts, we used a modified Poisson test, retaining only peaks with a probability $\leq$0.05 of arising from the same Poisson distribution as pre-peak charcoal counts. Return intervals were calculated as the average period between fires across the record and for specific intervals. Model validation employed the SNI (Signal to Noise Index) (Kelly et al., 2011), ensuring SNI >3 to accurately distinguish fire events from noise. In summary, a robust lowess model with a local threshold of 0.95 was constructed, balancing peak detection and frequency estimation.

2.5.4. Bacterial brGDGT-based temperature reconstruction

Given the poor pollen preservation in an important part of the sequence, brGDGTs were used as an independent continental palaeothermometer (e.g., Schouten et al., 2013; Inglis et al., 2022; McClymont et al., 2023). Branched GDGTs are ubiquitous membrane-spanning lipids with diverse numbers (4–6) and positions (5′, 6′, or 7′) of methyl groups and up to two cyclopentane rings (Fig. S2; Schouten et al., 2000; Sinninghe Damsté et al., 2000; Weijers et al., 2006; De Jonge et al., 2013, 2014; Ding et al., 2016). These membrane-spanning lipids are synthesised by heterotrophic bacteria (Weijers et al., 2006, 2009; Sinninghe Damsté et al., 2011, 2014, 2018; Chen et al., 2022; Halamka et al., 2023). Correlations of the Methylation of Branched Tetraethers index with temperature (Weijers et al., 2007; Peterse et al., 2012), notably after a restriction of this methylation index to brGDGTs with methyl groups at 5′ positions (MBT'$_{5ME}$; De Jonge et al., 2014), enables the use of brGDGTs and their derived MBT'$_{5ME}$ index as temperature proxies in all environmental settings (e.g., Raberg et al., 2022). The correlations between MBT'$_{5ME}$ and temperature likely reflect the ability of brGDGT-producing bacteria to adjust their membrane composition in

response to environmental conditions (Naafs et al., 2021).

Temperature-calibrations based on MBT'_{5ME} were established for soils (De Jonge et al., 2014; Naafs et al., 2017a; Dearing Crampton-Flood et al., 2020), peats (Naafs et al., 2017b; Dearing Crampton-Flood et al., 2020), and lake sediments (Russell et al., 2018; Martínez-Sosa et al., 2021). While soil and peat datasets may be grouped together for brGDGT–based calibrations (Dearing Crampton-Flood et al., 2020), lake sediments require distinct brGDGT–based calibrations (Martínez-Sosa et al., 2021). To assist the choice of an adequate brGDGT–based calibration for the ARE sequence, the Branched and Isoprenoid GDGT Machine learning Classification (BIGMaC) algorithm (Martínez-Sosa et al., 2023) was used to predict depositional environments from the GDGTs' perspective. All ARE samples were classified as soil samples, except one sample at 27.5 cal ka BP (level 451 cm) and two samples at c. 12.8 cal ka BP (levels 275 and 270 cm) which were classified as lake samples. However, the BIGMaC algorithm disregards contextual information from GDGT-independent proxies. Indeed, GDGT-independent records suggest seasonal ponds rather than permanent lakes (see sections 2.1.2 and 4.1) and lack of planktic diatoms, in agreement with the ARE sample classifications as soil samples but not those as lake samples. Furthermore, brGDGT distributions in ARE samples differ from those in most globally distributed surface soils and peats ($n = 1885$; Raberg et al., 2022; Häggi et al., 2023), notably in terms of brGDGT cyclisation degrees (Fig. S3). This discrepancy suggests that the training and testing datasets for the BIGMaC algorithm do not consider the peculiar brGDGT distributions in the ARE samples, and possibly the rest of the Canary Islands as well. Accordingly, a brGDGT–based calibration established for soils should be employed for this study, including for the ARE samples classified as lake samples by the BIGMaC algorithm.

Due to the absence of regional brGDGT–based calibrations for the Canary Islands, the following global soil calibration was employed: Mean annual air temperature $= 40.01 \times MBT'_{5ME} - 15.25$ ($n = 350$, $R^2 = 0.60$, root mean square error = 5.3 °C; Naafs et al., 2017a). Despite inherent uncertainties of approximately 5 °C for temperature (1σ) at the global scale (De Jonge et al., 2014; Naafs et al., 2017a), the selected global calibration was deemed suitable for the study, as the most recent brGDGT-based temperatures agree with the modern mean annual temperature of 20 °C within uncertainties (see Supplementary text 2 for further details on calibration selection, and Fig. S2–S4). Using the selected global calibration, both instrumental and analytical uncertainties translate to a 0.5 °C (1σ) uncertainty, which is similar to the inter-laboratory dispersion (offsets of 0.3–0.9 °C from the median; De Jonge et al., 2024a).

Instrumental and analytical uncertainties reflect the precision of brGDGT analyses, whereas calibration uncertainties reflect the dispersion of temperature calibrations attributable to seasonal and non-thermal biases in brGDGT-based temperatures (see sections 4.1 and 4.3 for a few examples). Given that such biases show a spatial variability which is partly due to contrasting environmental conditions (De Jonge et al., 2014; Naafs et al., 2017a; Dearing Crampton-Flood et al., 2020; and references therein), the cumulative effect of all biases at the global scale may not apply to the ARE sedimentary sequence and other sites in the Canary Islands. The global calibration error should thus be treated as an upper-bound of the dispersion that would be observed by constructing a local calibration through comparison of instrumental temperature and proxy variations over an extended period at a specific site (Davtian et al., 2019), whatever the environmental context. This caveat implies that even downcore changes in proxy-based temperatures smaller than their calibration uncertainty may hold palaeoclimatic and palaeoenvironmental significance, especially if these downcore changes agree with expected trends based on independent temperature records and/or temperature records from other sites subject to similar conditions. To assess the significance of downcore brGDGT-based temperature changes, analytical uncertainties rather than calibration uncertainties are used, as per Davtian et al. (2019).

3. Results

The age-depth model results indicate that the record spans between c. 27,530 cal a BP (level 250 cm) and c. 1390 cal a BP (level 50 cm), with an average resolution of 65 yr/cm, but showing stark changes in sedimentation rate (see result subsections). The Bacon model path overlaps all radiocarbon dates except for Beta_690055 (level 149 cm), likely an inversion due to old carbon redeposition (see Supplementary text 1 for additional age-depth model discussion). To provide an overview of the results based on the analysis of multiple indicators studied, the presentation and discussion of the results have been structured into sections that cover the six Northern Hemisphere climatic periods represented by the ARE sedimentary sequence.

3.1. Pre-Last Glacial Maximum (pre-LGM): zone ARE-1 (27.5–26 cal ka BP, 450–400 cm)

The pre-LGM period is represented by the 450–400 cm section of the ARE record (27.5–26 cal ka BP). The Bacon age-depth model indicated that the sedimentation rate in this section is 32 yr/cm on average. With a median particle size of 6.5 μm, granulometric data show a high silt content of up to 84 %, and low organic content (lowest of the record at 2.6 % in level 430 cm, 26.9 cal ka BP). Geochemical analysis (XRF) shows stable K (Potassium) concentrations at 0.9 %, stable Ti (Titanium) concentrations at 1.7 %, and stable Ca (Calcium) concentrations with a peak of 1.1 % at 410 cm (26.3 cal ka BP) (Fig. 2).

Between 450 and 440 cm (27.5–27 cal ka BP), *Morella faya* exhibits a high pollen abundance, peaking at 86 % and progressively declining to an average of 5.8 % between 430 and 400 cm (26.9–26 cal ka BP). *Pteris* fern spores also exhibit a sharp decline; they made up 51 % of the total pollen between 450 and 440 cm (27.5–27 cal ka BP), but only 11.4 % between 430 and 400 cm (26.9–26 cal ka BP), and zygospores of *Spirogyra* are present. The percentage of *Pinus canariensis* pollen increases from 6 % to 13 % between 450 and 440 cm (27.5–27 cal ka BP) to an average of 39 % between 430 and 400 cm (26.9–26 cal ka BP). Between 450 and 440 cm (27.5–27 cal ka BP), Cyperaceae pollen increases from 11.2 % to 47 % at its peak. The maximum concentration of *Pteris* spores is recorded at 440 cm (27 cal ka BP) with 68,000 spores/cm^3 (Fig. 3).

Macrocharcoal analysis showed variations, with lower concentrations (85 particles/cm^3) between 420 and 400 cm, peaks exceeding 1000 particles/cm^3 between 440 and 420 cm (27–26.6 cal ka BP), and low abundance between 460 and 440 cm (27.8–27 cal ka BP). Microcharcoal concentrations are very low between 450 and 430 cm, averaging 136 particles/cm^3, and rise to an average of 8000 particles/cm^3 between 420 and 400 cm. CharAnalysis identifies two fire events, with a return interval of 380 years, the first at 27 and 26.7 cal ka BP (Fig. 4). Air temperature estimates based on branched GDGTs (brGDGTs) increase from 8.2 to 14.8 °C. According to the pollen-based climate model, these were the highest levels of humidity and precipitation on record (reaching up to 75 % and 756 mm respectively), with temperatures hovering around 14 °C and dropping to 13.1 °C at the end of the period (Fig. 5).

3.2. Last Glacial Maximum (LGM): zone ARE-2 (26–14.5 cal ka BP, 400–337 cm)

The sedimentation rate in the Arucas basin in this period (c. 26–14.5 cal ka BP) is on average 180 years/cm showing an increasing trend (progressively slower sedimentation). With a median particle size of 5.6 μm, the percentage of silt is stable at 78 %. At 380 cm (c. 23 cal ka BP), the Ca concentration stays constant at 14.4 %. Ti content is stable at 2 %, with an average XRF value of 13 % at 360 cm (c. 20 cal ka BP). Concentrations of sand remain stable, and between 390 and 340 cm, K concentration drops to 0.6 %, and at level 340 cm, rises to 1 %, and the ratio K/Ti shows increased values. Al (Aluminium) content rises between 390 and 350 cm (c. 25–17.9 cal ka BP) (Fig. 2).

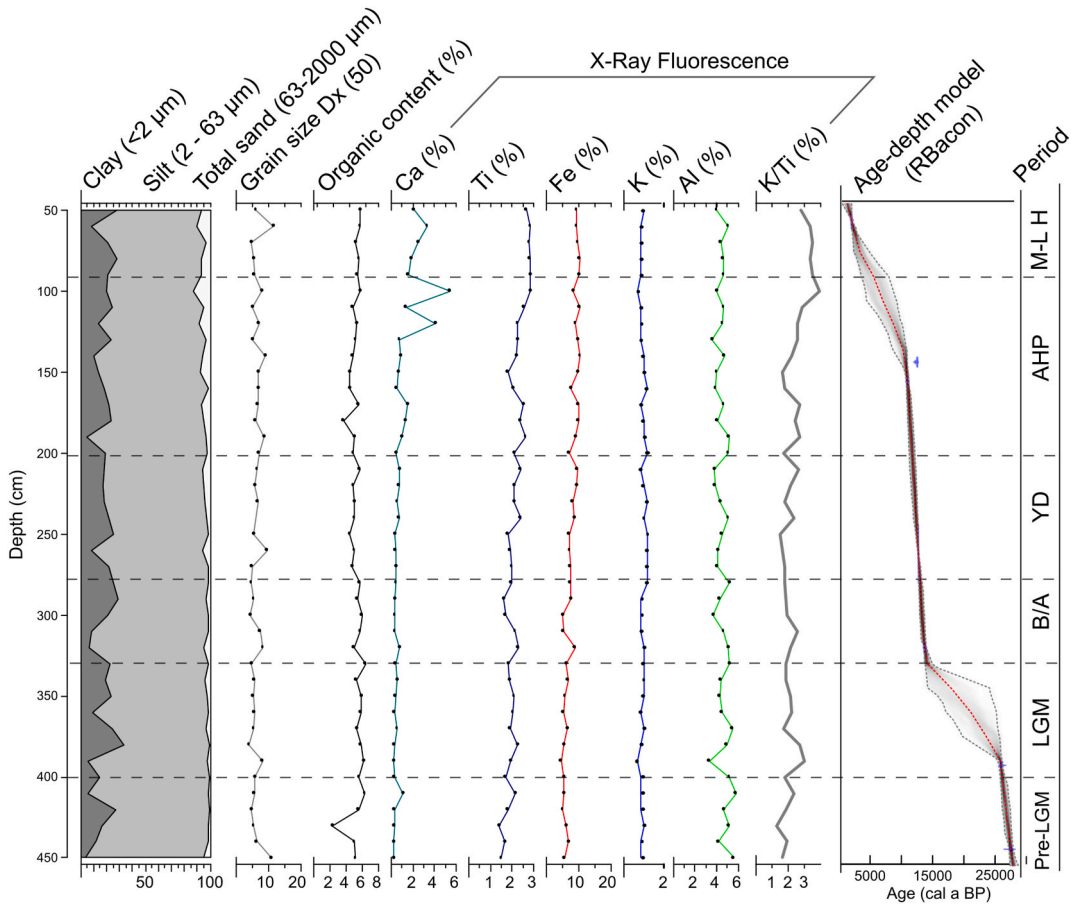

Fig. 2. Selected sedimentological data of the Vega de Arucas sedimentary sequence (ARE) in Gran Canaria, with depth (cm), and summary of Bayesian age-depth model. Periods in the right margin: Pre–LGM: pre-Last Glacial Maximum (30–26 cal ka BP), LGM: Last Glacial Maximum (c. 26–14.5 cal ka BP), B/A: Bølling-Allerød (14.5–12.9 cal ka BP), YD: Younger Dryas (12.9–11.7 cal ka BP), AHP: Early Holocene/African Humid Period (11.7–5 cal ka BP), M-LH: Middle and Late Holocene (5 cal ka BP–present).

Pollen preservation remains sufficient for pollen identification, but concentrations are lower than in the previous section (average 7414 pollen/cm^3). *Pinus canariensis* pollen is dominant, averaging 62 % and peaking at 89 % at 360 cm (c. 19.5 cal ka BP), while *Morella faya* remains low. Proportions of pollen from *Erica* are stable at 1 % and peak at 8 % at 370 cm (c. 22 cal ka BP). Cyperaceae pollen averages 25 % between 390 and 370 cm (c. 25–22 cal ka BP), decreasing to 4.5 % between 360 and 340 cm (20–15.5 cal ka BP). At 9.2 % on average, Asteraceae pollen proportions are stable. *Pteris* spores peak at 52 % at 390 cm, with an average of 14 %. Zygospores of *Spirogyra* are more prevalent (3 %), falling to 0.8 % between 360 and 330 cm (c. 20–15.5 cal ka BP). Spores of Polypodiaceae ferns increased, on average, by 4.1 % in comparison to the previous zone (Fig. 3).

Macrocharcoal concentrations vary from approximately 80 particles/cm^3 at 400–342 cm (c. 26–16 cal ka BP). Averaging less than 5000 particles/cm^3, microcharcoal concentration is low, except peaks at 350 cm (c. 17.9 cal ka BP). Despite achieving SNI >3, the CharAnalysis model designed for 320–394 cm yielded no positive fire detections, likely due to abruptly changing sedimentation rates (Fig. 4). Branched GDGTs yield temperature estimates of around 14 °C. According to the pollen climate model, relative humidity ranges from 50 % to 70 %, precipitation ranges from 487 to 622 mm, and average temperatures fall between 13.5 and 14.6 °C (Fig. 5).

3.3. Bølling-Allerød (B/A): zone ARE-3 (14.5–12.9 cal ka BP, 336–277 cm)

The sedimentation rate speeds up, reaching an average of 30 years/cm in the B/A period (14.5–12.9 cal ka BP). The concentration of clay varies; it reaches 7 % between 320 and 310 cm and rises noticeably to 24 % between 300 and 277 cm (14–12.9 cal ka BP). The XRF geochemical data exhibit stable values, except for Ti (%) and Fe (Iron) (%) increases at the start of the zone (Fig. 2).

Pinus canariensis pollen proportions show decreasing trend during this period, from dominant (62 %) between 330 and 290 cm, to declining to 10.7 % by level 280 cm (13 cal ka BP), while Asteraceae shows stark increases after this level (up to 35 %). The pollen content of *Juniperus* increases, reaching 2.4 % at 310 cm (13.5 cal ka BP) and 7.4 % at 280 cm (13 cal ka BP). Only at 320 cm (13.6 cal ka BP) are *Spirogyra* zygospores present. *Pteris* spores increase to 28 % between 320 and 300 cm (13.6–13.3 cal ka BP), then fall to 8.5 % between 290 and 280 cm (c. 13 cal ka BP). Polypodiaceae fern spores peak at 9 % at level 320 cm (13.6 cal ka BP). Spores of monolete ferns show a peak at 310 cm (13.5 cal ka BP) (Fig. 3).

The record's highest concentration of macrocharcoal particles (617 particles/cm^3) is found at the beginning of this period: between 330 and 324 cm (14–13.7 cal ka BP), macrocharcoal concentration values are >300 particles/cm^3. Then microcharcoal particles decrease until level 296 cm (13.2 cal ka BP, 73 particles/cm^3 on average) and finally increase (average 161 particles/cm^3) until the end of the zone. Microcharcoal exhibits high values between 320 and 310 cm (13.5–13.4 cal ka BP), peaking at 280 cm (25,000 particles/cm^3). A total of three fire events are found (13.2, 13 and12.9 cal ka BP), and return intervals are 164 and 82 years (Fig. 4).

Branched GDGT-based temperatures fluctuate, with a maximum of 16.7 °C at 300 and 280 cm (13.2–13 cal ka BP), and a minimum of 11.8

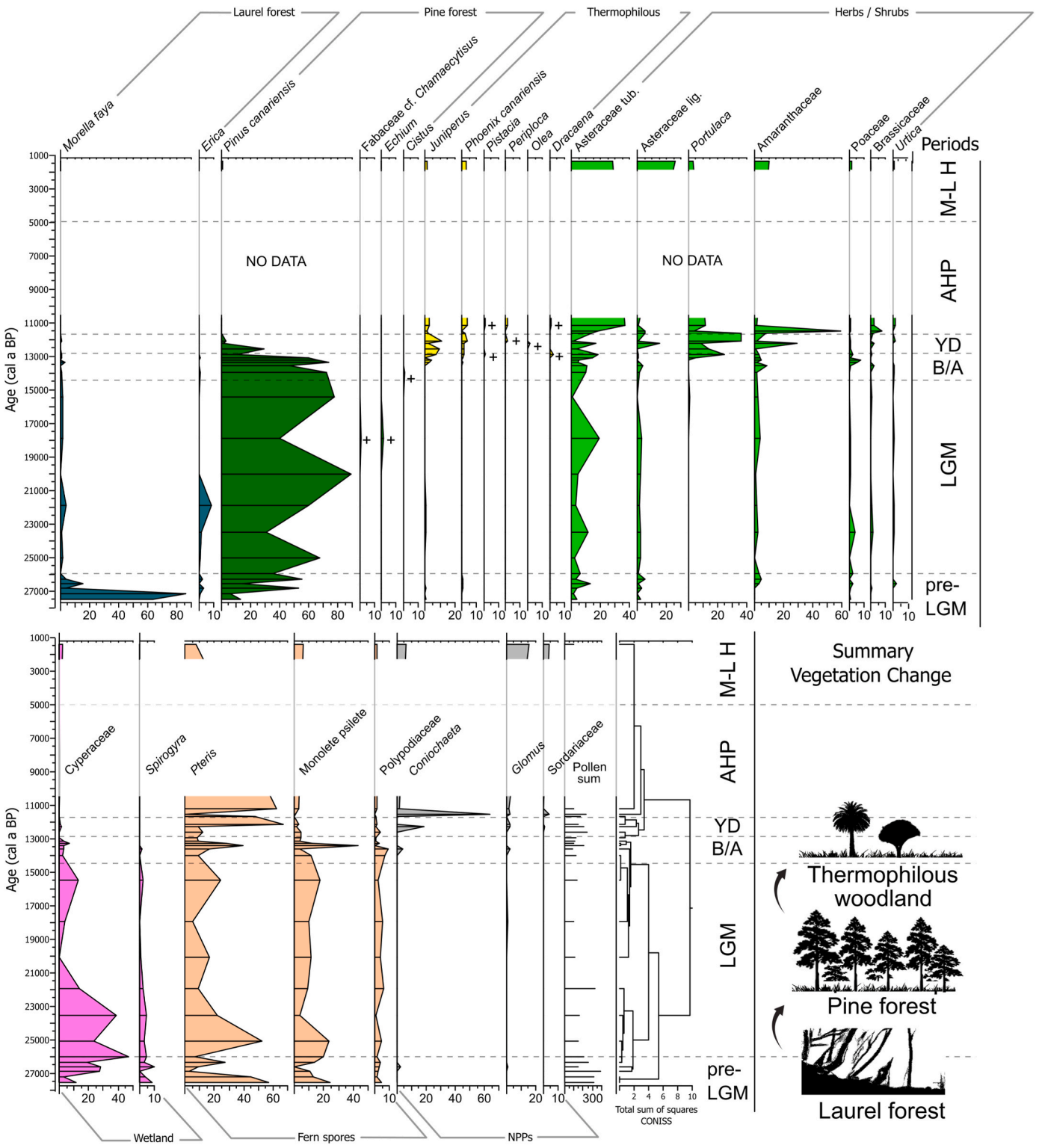

Fig. 3. Diagram of microfossils (charcoal, diatoms, selected pollen arranged by vegetation type, and ferns and fungal spores) of the sedimentary sequence of Vega de Arucas (ARE) in Gran Canaria. The black crosses indicate presence of pollen in samples <1 %. The results are presented in relation to age (cal a BP). Pre–LGM:pre-Last Glacial Maximum (30–26 cal ka BP), LGM: Last Glacial Maximum (c. 26–14.5 cal ka BP), B/A: Bølling-Allerød (14.5–12.9 cal ka BP), YD: Younger Dryas (12.9–11.7 cal ka BP), AHP: Early Holocene/African Humid Period (11.7–5 cal ka BP), M-LH: Middle and Late Holocene (5 cal ka BP–present).

°C at 270 cm (12.8 cal ka BP). The pollen climate model suggests increasing temperatures between 13.0 and 17.7 °C, with decreasing precipitation (down to 302 mm by 12.9 cal ka BP), and relative humidity values between 50 % and 60 % (Fig. 5).

3.4. Younger Dryas (YD): zone ARE-4 (12.9–11.7 cal ka BP, 277–203 cm)

The sedimentation rate in zone ARE-4 (YD, 12.9–11.7 cal ka BP) is c. 16 years/cm. Sand peaks with a median particle size of 7 μm are found at

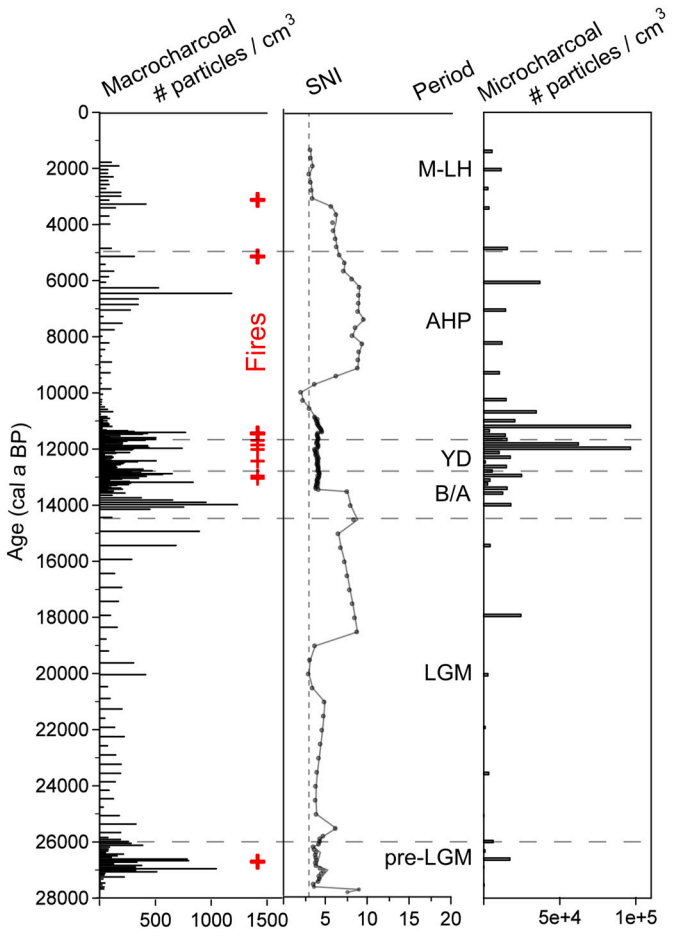

Fig. 4. Diagram of macro- and microcharcoal in the sedimentary sequence of Vega de Arucas (ARE) in Gran Canaria. The red crosses on the charcoal curve indicate fire events identified with CharAnalysis and the grey dashed line indicates the SNI (Signal to Noise Index). The results are presented in relation to age (cal a BP). pre-LGM:pre-Last Glacial Maximum (30–26 cal ka BP), LGM: Last Glacial Maximum (c. 26–14.5 cal ka BP), B/A: Bølling-Allerød (14.5–12.9 cal ka BP), YD: Younger Dryas (12.9–11.7 cal ka BP), AHP: Early Holocene/African Humid Period (11.7–5 cal ka BP), M-LH: Middle and Late Holocene (5 cal ka BP–present). (For interpretation of the references to colour in this figure legend, the reader is referred to the Web version of this article.)

depths of 260 cm (12.6 cal ka BP), 220 cm (12 cal ka BP), and 210 cm (11.8 cal ka BP). Fe proportions show an increase, ranging from 7 % to 9.5 % and reaching a peak of 16.5 % at 210 cm (11.8 cal ka BP), and Ti proportions rise overall from 1.9 % to 2.4 %. Ca content increases from 0.4 % to 0.8 % with a maximum of 0.7 % at 212 cm. K and Al proportions, on the other hand, show a declining trend (Fig. 2).

Pollen from *Pinus canariensis* drops from 30 % at 260 cm (12.6 cal ka BP) to 3 % at 240 (12.3 cal ka BP). While other species remain stable, *Juniperus* pollen exhibits notable peaks of 9 % at 260 cm (12.6 cal ka BP) and 11 % at 230 cm (12.1 cal ka BP). The proportion of Asteraceae pollen is 37 % on average, with *Portulaca* showing an increase from 13 % to 36 %. At present, *Portulaca canariensis* is the only native species of this genus, making it the most likely candidate. Pollen of the Amaranthaceae family reaches its peak at 29 % at 240 cm (12.3 cal ka BP). *Pteris* spores peak at 67 % in level 230 cm (12.1 cal ka BP), where *Periploca* pollen is present. No *Spirogyra* zygospores are found in this zone (Fig. 3).

The average value of macrocharcoal concentrations in the 264–236 cm (12.7–12.3 cal ka BP) section is approximately 148 particles/cm^3, which decreases in the 234–220 cm section (12.3–12 cal ka BP) before increasing to an average of 145 particles/cm^3 until 11.7 cal ka BP. The microcharcoal curve exhibits mean concentrations of 11,000 particles/cm^3 between 260 and 230 cm (12.6–12.1 cal ka BP), reaching values of up to 96,000 particles/cm^3 at 220 and 210 cm (11.9–11.8 cal ka BP). According to the CharAnalysis, there were three fires (12.4, 12, and 11.8 cal ka BP), with 533, 410, and 164-year return intervals, respectively (Fig. 4).

Temperature estimates derived from brGDGTs oscillate between 9 and 17.2 °C. Average temperatures according to the pollen climate model are also between 13.8 and 16.8 °C, with a relative humidity of roughly 60 %, and some of the lowest precipitation values of the record (down to 270 mm c. 12 cal ka BP) (Fig. 5).

3.5. Early Holocene/African Humid Period (AHP): zone ARE-5 (11.7–5 cal ka BP, 202–92 cm)

The sedimentation rate is c. 60 years/cm in this period, showing a trend towards slower sedimentation (c. 11.7–5 cal ka BP). Granulometry shows stable proportions of clays c. 20 %, and sand increases, with an average particle size of 7.4 μm and peaks of about 7 % between 170 and 150 cm (c. 11.2–10.1 cal ka BP). Fe content oscillates c. 9 %, and the percentage of organic matter stays at 14.7 % on average. The amount of Ca shows peaks of 1.4 % at 180 cm (c. 11.3 cal ka BP) 170 cm (11.2 cal ka BP), and above 4 % at 120 cm (c. 7.4 cal ka BP) and 100 cm (5.6 cal ka BP) (Fig. 2). The concentration of Ti shows an upward trend, rising from 2.3 % to 2.9 %, and K values stay low, averaging 0.8 %. This is reflected on higher values in the K/Ti ratio at the end of the zone, Al concentrations are consistent, oscillating c. 4.2 % (Fig. 2).

Pollen from *Erica* and *Morella faya* is scarce, and *Pinus canariensis* is rare in any of the samples between 200 and 170 cm (11.7–11.2 cal ka BP), but Asteraceae (tubuliflorae and liguliflorae types) pollen is abundant with an average of 45 %. Pollen from *Juniperus* and *Phoenix* is present, and the proportions of *Portulaca* pollen decrease down to 4 %. The pollen of Amaranthaceae shows a notable peak of 59 % at 190 cm (c. 11.5 cal ka BP) and then falls to 2 % at 170 cm (c. 11.2 cal ka BP), when *Periploca* pollen is present. *Pteris* fern spores increase up to 63 % at 170 cm (c. 11.2 cal ka BP). *Coniochaeta* fungal spores are detected, accounting for 64 % over the total pollen, at 190 cm (11.5 cal ka BP) (Fig. 3). From 170 cm onwards the pollen record is the pollen is so deteriorated that the analysis is restricted to recording the presence of degraded Amaranthaceae and Asteraceae pollen grains. The spores of *Pteris* fern are also found in small quantities, less than 7000 spores/cm^3 in all samples.

The macrocharcoal concentration exhibits a decreasing trend with an average of 186 particles/cm^3 between 202 and 184 cm (c. 11.7–11.4 cal ka BP), and lower values averaging 63 particles/cm^3 between 184 and 138 cm (c. 11.4–9 cal ka BP). Four fires are found by CharAnalysis (c. 11.6, 11.4, 6.8, 5.1 cal ka BP) (Fig. 4). The microcharcoal values in the rest of the zone vary below 40,000 particles/cm^3, with a peak concentration of 96,000 particles/cm^3 observed at 170 cm (11.2 cal ka BP).

The average temperature estimated from brGDGTs is 15.7 °C. The pollen climate model infers temperatures between 14.9 and 18.0 °C, relative humidity above 60 %, and precipitation between 298 and 361 mm between c. 11.7–11.2 cal ka BP (Fig. 5).

3.6. Middle and Late Holocene (M-LH): zone ARE-6 (5–1.2 cal ka BP, 92–50 cm)

A sedimentation rate of 90 years/cm is estimated based on the age-depth model in zone ARE–6 (M-LH, c. 5–1.2 cal ka BP). Sand-sized particles show an average of 7 % in this zone, and the median particle size is 6.7 μm. A relatively stable organic matter content is recorded, with an average of 8.5 %. Elements like Ti have an increasing trend in percentage, reaching 2.8 %, and Fe maintains high concentrations, averaging 9.6 %. Ca and Al proportions are stable, with average values of 2.3 % and 4.5 %, respectively, whereas K proportion shows a decrease to c. 0.8 % (Fig. 2).

Asteraceae types make up a large percentage of the only sample

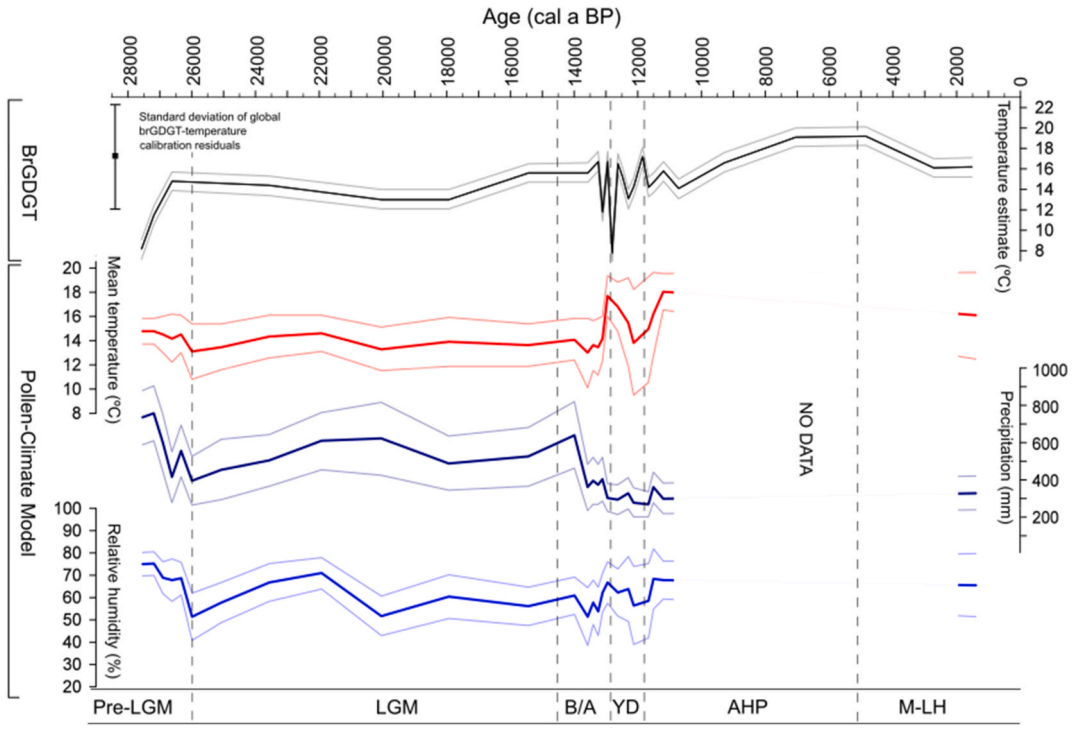

Fig. 5. Plot of temperature reconstruction from brGDGT (branched glycerol dialkyl glycerol tetraether) distribution with analytical SD error, and temperature, relative humidity, and precipitation reconstruction from the pollen climate model of the Vega de Arucas sedimentary sequence (ARE) in Gran Canaria. Error 0.5(%). The results are presented in relation to age (cal a BP). pre-LGM: pre-Last Glacial Maximum (30–26 cal ka BP), LGM: Last Glacial Maximum (c. 26–14.5 cal ka BP), B/A: Bølling-Allerød (14.5–12.9 cal ka BP), YD: Younger Dryas (12.9–11.7 cal ka BP), AHP: Early Holocene/African Humid Period (11.7–5 cal ka BP), M-LH: Middle and Late Holocene (5 cal ka BP–present).

showing pollen preservation (64 %), at 50 cm (Fig. 3). *Juniperus*, *Phoenix canariensis*, and *Pinus canariensis* are also scarcely present. Furthermore, many spores of the mycorrhizal fungi *Glomus* type are found. In general, macroscopic charcoal values are low (less than 100 particles/cm^3), peaking between 82 and 80 cm (c. 3.5 cal ka BP), with 208 particles/cm^3. One fire event is detected c. 3.1 cal ka BP (Fig. 4).

Three samples allow for the calculation of temperature estimations through brGDGTs, with the first one at 19.2 °C, similar to the previous period, while the last two exhibit values of 16.1–16.2 °C. The average temperature, relative humidity, and amount of rainfall for the upper pollen sample are 16.1 °C, 65.44% and 327 mm respectively (Fig. 5).

4. Discussion

4.1. Pre-Last Glacial Maximum (pre-LGM, 28–26 cal ka BP)

Pollen data indicates that pre-LGM vegetation in the Vega de Arucas was dominated by laurel forest species. In addition, the presence of indicator species such as *Morella* and low fire activity (Fig. 3, Fig. 4) are noteworthy, as they imply that, by contrast to the present, laurel forest would have developed at substantially lower elevations, around 200 m below its predicted potential lower limit and 400 m below its current distribution during this time (del Arco et al., 2006). Based on the fidelity (matching occurrences of pollen and parent plants) and dispersibility (pollen presence without corresponding plant presence) values measured in modern pollen rain, *Morella faya* pollen is considered a reliable indicator of the nearby presence of its parent trees (de Nascimento et al., 2015). However, at the regional (island) scale, its pollen can be dispersed into adjacent communities, and transport is common, from the laurel forest upward to the pine forest and further to the summit scrub, while downward transport is less evident. *Pinus* pollen is also a good indicator of local presence, as it is well represented in pine forest stands. Although some pollen transport occurs, the contribution of non-locally sourced pollen types is generally low. Currently, *Morella* pollen percentages in the laurel forest range between 10 % and 69 %, compared to 0–29 % in pine forests and 1–26 % in thermophilous woodlands (de Nascimento et al., 2015). Notably, during the pre-LGM, *Morella* pollen reached up to 86 % in the fossil record, exceeding present-day levels in laurel forests. This suggests a strong local presence and dominance of the species at that time. By contrast, the pollen percentages for other indicators such as *Pinus* (6–13 % during the pre-LGM vs. 20–86 % today) and *Juniperus* (0.3 % vs. 1–25 % today) do not match the levels expected from their modern vegetation communities (de Nascimento et al., 2015), further suggesting that their pollen was likely transported from more distant upper or lower vegetation belts during that period. At the end of the zone (c. 27 cal ka BP) a transition to pine forest occurs, and fire activity increases. This suggests that either climate change, marine transgressions or both have caused altitudinal redistributions of ecosystems during this period.

The Mediterranean climate with its consubstantial seasonality developed approximately 3 million years ago, at the onset of the Pleistocene glaciations (Suc, 1984), and the summer dry season has since presented the most relevant constraint on Canary Island vegetation. In the case of laurel forests, which are cloud forests relying on constant moisture supply (Fernández-Palacios et al., 2017), the presence of sea clouds during the summer—currently sustained by trade wind-driven cloud cover—is the sole factor enabling them to endure the dryness. Currently, laurel forest in the Canary Islands (where the laurel forest pollen signal predominates; de Nascimento et al., 2015) develops between 600 and 1200 m a.s.l. in areas with average annual precipitation between 500 and 1200 mm and an annual average temperature range of roughly 13–18 °C (del Arco and Rodríguez Delgado, 2018). According to the pollen climate model, the establishment of a laurel forest at a lower elevation, such as in the Vega de Arucas corresponds to a 4 °C decrease in relation to current temperatures. By contrast, temperatures inferred from brGDGTs, ranging from 8.2 to 11.5 °C during laurel forest species

dominance with little fire activity, are lower than those estimated for the LGM (13–14 °C), when global cooling averaged −6.1 °C (Tierney et al., 2020), and are similar to temperatures inferred from pollen only during the transition to pine forest with accompanying fire activity. However, the brGDGT signal is not only temperature-dependent, as it can also be affected by other variables such as nearby vegetation and waterlogging (e.g., Menges et al., 2014; Dang et al., 2016; Davtian et al., 2016; Liang et al., 2019; Duan et al., 2022; De Jonge et al., 2024b). These other variables, which are mostly non thermal factors, contribute to the global brGDGT–based calibration uncertainties of roughly 4–5 °C (De Jonge et al., 2014; Naafs et al., 2017a; Dearing Crampton-Flood et al., 2020). Thus, the pre-LGM in Vega de Arucas experienced possibly colder climates as well as wetter summers (maybe along with a lower sea of clouds) or more precipitation than in current times, that allow the presence of seasonal ponds (as evidenced by zygospores of *Spirogyra*) and the occurrence of a laurel forest at lower elevations.

Such pollen-inferred pre-LGM precipitation and vegetation conditions may partly explain the relatively low pre-LGM brGDGT-based temperatures, as brGDGTs directly record soil rather than air temperatures (e.g., Wang et al., 2016, 2020; Pérez-Angel et al., 2020), which may yield systematic biases due to soil-air temperature offsets (e.g., Smerdon et al., 2004; Lembrechts et al., 2022; Molnar, 2022). As evidenced by seasonal ponds, increased precipitation likely resulted in moister soils with increased heat capacity compared with drier soils, which yields lower soil-air temperature offsets and thus possibly lower brGDGT-based temperatures despite constant or increasing air temperature (e.g., Guo et al., 2024, 2025). Alternatively, increased precipitation and resulting seasonal ponds yielded a soil moisture effect on brGDGTs for other reasons than changes in soil heat capacity, as the soil moisture effect on brGDGTs may occur next to or within a water body even in case of unchanged precipitation (Dang et al., 2016). Changes in vegetation cover and type may also affect brGDGT-based temperature reconstructions, for instance via shading—which reduces soil-air offsets—and vegetation-related changes in soil properties and brGDGT-producing bacterial communities (e.g., Davtian et al., 2016; Liang et al., 2019, 2023; Lu et al., 2019). Indeed, brGDGT distributions during laurel forest predominance show the most peculiar patterns in terms of cyclisation degrees compared with global surface soils and peats (Fig. S3b).

Because of their anemophilous or mixed pollination mode, *Morella* and *Erica* are usually overrepresented in laurel forest pollen records over other entomophilous species that are dominant (e.g., Lauraceae trees) (de Nascimento et al., 2015). Both are pioneer trees which are highly abundant in secondary succession stages, however, *Erica* is more abundant at early succession stages while *Morella* persists within mature forests (Fernández-Palacios et al., 2017). The low representation of *Erica*, a heliophilous taxon, strongly indicates a closed forest environment (de Nascimento et al., 2015; del Arco and Rodríguez Delgado, 2018). Additionally, the occurrence of *Pteris*, with *Pteris incompleta* being the only native *Pteris* species in the Canary Islands, supports the idea of a humid laurel forest, as it is currently rare and stands near watercourses (Bañares et al., 2004). It is possible that, rather than an extreme shift toward a humid laurel forest, a dry, thermophilic variant of the laurel forest may have developed instead. However, because most tree species in the laurel forest are entomophilous and thus, underrepresented in pollen records, differential pollen preservation prevents us from knowing the exact type of laurel forest that developed in this region (see de Nascimento et al., 2015). Either way, the existence of laurel forest, in any form, suggests that water was available during the dry season, outcompeting the thermophilous woodlands that currently typically grow at these elevations.

During the pre-LGM, changes in vegetation patterns are closely linked to fluctuations in fire frequency and intensity. Only one fire event is found in the ARE record when the laurel forest pollen signal predominates. The transition to a drier pine forest with more biomass, as indicated by higher *Pinus* pollen and lower *Morella*, resulted in an increase in fire frequency. This evidence suggests that the laurel forest existing prior to the LGM experienced infrequent natural fires, like those observed in the fossil record from the La Gomera millennia ago (Nogué et al., 2013).

4.2. Last Glacial Maximum (LGM, 26–14.5 cal ka BP)

During this period the record has a low resolution due to a stark decrease in sedimentation rate (180 yr/cm). The pollen data suggest that between c. 27–25 cal ka BP, the laurel forest in Arucas was replaced by a pine forest. Currently, the Canary Island pine forest grows between 1200 and 2000 m a.s.l., on windward slopes, and between 800 and 2200 m a.s.l., on leeward slopes, with average annual temperatures of 11–15 °C, and highly variable annual rainfall between 400 and 1000 mm (del Arco and Rodríguez Delgado, 2018). This suggests that cooler temperatures than those experienced today would have increased the pine forest community's competitiveness in comparison to thermophilous woodlands or laurel forests. Moreover, at present, *Morella* is usually found in the understory of pine forests with sufficient moisture, but it is absent in drier pine environments (Salas et al., 1998). Therefore, the decline in *Morella* suggests that this community was probably analogous to a current dry pine forest.

The Last Glacial Maximum (LGM) is central to most hypotheses around the past climate of the Canary Islands. According to global estimates, temperatures would have been 6 °C lower than they are now, and the sea level 125–130 m lower than it is today (Clark and Mix, 2002; Tierney et al., 2020), which could cause ecosystems to shift altitudinally towards lower zones and benefit vegetation that is adapted to colder conditions. Indeed, our pollen-based climate models in ARE estimate a mean temperature drop to about 14 °C, while brGDGTs indicate an increase by roughly 2 °C compared to pre-LGM estimates, followed by LGM estimates similar to those from pollen-based climate models within uncertainties. Future local brGDGT calibration studies may help confirm whether the pre-LGM colder climate indication is accurate, or if it is influenced by the vegetation canopy effect or regional variations (Pérez-Angel et al., 2020).

According to von Suchodoletz et al. (2010), there was higher atmospheric humidity in the Canary Islands during the LGM than during the current interglacial period, as shown by proxies such as clay content and magnetic susceptibility in aeolian sediments from Lanzarote. They propose two scenarios: precipitations increased due to intensive winter cyclones originating in the North Atlantic, or a northward shift in the Intertropical Convergence Zone that led to a migration of the West African Monsoon into the latitudes of the Canary Islands (von Suchodoletz et al., 2010). Regarding vegetation changes, Fernández-Palacios et al. (2016) suggest that temperature drops, marine regressions, and glaciation effects resulted in a vertical realignment of vegetation zones, which in turn caused species adapted to cooler climates to shift to lower elevations. The ARE record demonstrates the loss of *Morella* from the area during the LGM. *Morella* is also native to humid pine forests and can withstand low temperatures. This indicates a reduced water availability, which is supported by a decrease in *Spirogyra* algae zygospores, indicating reduced waterlogging. Low precipitation is also reflected in a decrease in sedimentation rate, dropping to less than 1 cm in over 150 years. This agrees with the global trend towards drier conditions during the LGM (Bartlein et al., 2011).

Another proposed idea is that throughout the pre-LGM period, the trade winds were stronger, carrying more Saharan dust (Zühlsdorff et al., 2007, 2008), a situation analogous to unusual modern observations of 'blood rains' in the Canary Islands (Criado and Dorta, 2003). This dust intrusion would have been especially acute during the Heinrich events, occurring immediately before and after the LGM (from Heinrich-6 at 60 cal ka BP to Heinrich-0 at 12 cal ka BP), connected with iceberg fleets drifting southward from the Laurentide and Fennoscandian ice sheets into the North Atlantic (Collins et al., 2013). Concurrently, it has been proposed that the Canary Current intensified,

further cooling the region (Moreno et al., 2002). Our sedimentological data does not show pronounced changes, making it difficult to test this hypothesis. However, marine sediment samples from halfway between the Canary Islands and Cabo Verde show an increase in pine pollen signal around 18 cal ka BP, interpreted as an increase in trade wind strength (Hooghiemstra et al., 2006). The increase in the pine pollen signal in marine records may have resulted from two primary sources: the Canary Islands or the Mediterranean basin. These changes likely reflect both the strengthening of the trade winds and a regional expansion of coniferous forests. The high abundance of pine pollen in the ARE record indeed suggests an expansion of pine forest at lower elevations, which, because of the islands' conical shape, translates into a multiplicative increase in the area covered by forest. Probably, elements of the laurel forest retreated to ravines or lower elevations where sufficient moisture remained available.

Contrary to expectations, the establishment of pine forests in the Vega de Arucas was not associated with an increase in fire frequencies. While charcoal analysis revealed occasional peaks, suggesting sporadic burning events, no sustained fire activity was detected. This challenges the common assumption that pine forest expansion typically leads to more frequent fires. Although it is unlikely that there were no fires, given the dynamics of the fire regime in the pine forest at present, this low frequency may have resulted from the low temperatures that affected ignition in the pine forest at that time. It must be noted that fire detection may be challenging due to the low temporal resolution in this zone (167 yr/cm). Even in areas with lower temperatures and coniferous forests, such as the boreal taiga, similar techniques reveal a higher fire frequency, with fire events occurring at intervals of less than 900 years (Feurdean et al., 2020; Mazei et al., 2020).

4.3. Deglaciation (Bølling-Allerød (B/A), 14.5–12.9 cal ka BP and Younger Dryas (YD), 12.9–11.7 cal ka BP)

Pollen analysis from Vega de Arucas indicates that during deglaciation, pine forests disappeared and were replaced by vegetation primarily dominated by junipers and palms, as well as herbaceous plants that are typical of an open thermophilous woodland. Pollen in this part of the record starts showing signs of deterioration, and some samples did not contain enough pollen grains for their analysis (levels 270, 250, 220, and 210 cm), and is fully absent or too deteriorated during the Holocene period (samples 160–60 cm). The degradation of palynomorphs in the uppermost sections of the record, and specially the upper 160 cm, is linked to sedimentary changes (increased median grain size, sand content and mineralogenic content reflected in higher titanium concentration) and the absence of aquatic indicators (zygospores of *Spirogyra*), suggesting that seasonal ponds ceased due to higher temperatures and decreased precipitation. These coarser, non-waterlogged sediments likely underwent a combination of processes such as microbial attack, oxidation and microfossil abrasion through mechanical forces (Havinga, 1967). These conditions did not affect the preservation of charcoal particles, as charcolified material is generally more resistant to physical and chemical decomposition (Caromano and Cascon, 2014).

The deglaciation process in Europe and North America started after the LGM and lasted c. nine millennia (Roberts, 2009). Unsteady temperature increases characterised this time lapse, with ice sheets periodically growing and retreating because of thermal fluctuations. These oscillations included warmer periods like the B/A (c. 15–12.9 cal ka BP) and cooling periods like the Oldest Dryas (c. 19–15 cal ka BP) and YD (12.9–11.7 cal ka BP). According to fossil evidence found in the Northern Hemisphere from beetles and chironomids, summer temperatures increased dramatically during the Bølling-Allerød and eventually reached or even surpassed modern levels (Bowen, 2009). Even though it is thought that Canary Islands temperatures stayed constant during the deglaciation (Yanes, 2008; Yanes et al., 2011), there was a noticeable variation between the wet and dry seasons. Arid periods are associated with climatic shifts in North Africa between 14.9 ± 3.6 ka and 11.0 ± 4.0 ka according to data from amino acid racemisation zones of sedimentary deposits (Ortiz et al., 2005). Furthermore, the Saharan dust deposits in Lanzarote imply that dry periods preceded Heinrich events, turning humid both during and after these occurrences (Heinrich et al., 2021). Similar humid phases were identified in Fuerteventura at approximately 17 and 15 ka cal BP. (Petit-Maire et al., 1987; Coello et al., 1999).

Our data show that the Canary Islands were strongly impacted by the deglaciation period. Even with the ocean's moderating influence, independent indicators in ARE show sudden and abrupt variations in temperature, humidity, vegetation altitudinal distribution, and fire regimes. Overlapping peaks and valleys (Figs. 2–6) show these variations. This time frame, which stands in stark contrast to the Holocene, reflects the difficulty of conclusively ending the LGM and beginning the present interglacial epoch. A landscape primarily dominated by open thermophilous woodland suggests temperatures ranging from 15 to 19 °C, with roughly 250–400 mm of precipitation (Fernández-Palacios et al., 2024). The pollen-based climate model also shows decreased precipitation, from 622 to 277 mm, and a general temperature increase, from 14 to 18 °C (Fig. 4) with oscillations. Notably, Amaranthaceae pollen, which is prevalent in Saharan vegetation and spread by easterly winds, predominates in several ARE samples dated approximately around the YD (Hooghiemstra et al., 2006). Although pollen production by native species of Amaranthaceae complicates definitive conclusions if this pollen is exogenous, it could indicate periods of increased dust deposition in the Canary Islands as some authors have suggested (Williams et al., 2016; Heinrich et al., 2021).

Temperatures inferred from brGDGTs oscillate between roughly 9 and 17 °C without any general trends, differently from pollen-based temperatures, and these oscillations occur after the vegetation change from pine forests to juniper, palms, and herbaceous plants. In addition to the precipitation and vegetation effects previously discussed in section 4.1, the reduced precipitation and more arid B/A and YD conditions relative to the LGM may challenge brGDGT-based temperature reconstructions (e.g., Dirghangi et al., 2013; Menges et al., 2014; Dang et al., 2016; Duan et al., 2020, 2022; Guo et al., 2022), resulting in larger calibration residuals for arid environments than for humid environments (De Jonge et al., 2014; Naafs et al., 2017a; Dearing Crampton-Flood et al., 2020). Indeed, the brGDGT-based temperature oscillations by up to roughly 8 °C during the B/A and YD fall within the 2σ global calibration uncertainties of roughly 8–10 °C. As previously discussed in section 4.2, a local brGDGT calibration is required to assess thermal and non-thermal effects—including vegetation, precipitation, and aridity—on brGDGTs in the Canary Islands.

After thousands of years without fires during the LGM, fire activity in Vega de Arucas resumed during the deglaciation. During the B/A, the highest concentrations of charcoal are found, with a rapid return interval (170 years), while in the YD, the fire return interval increases to over 442 years. Changes in seasonality causing more ignition events, rising temperatures, or the transition of vegetation and biomass could have contributed to this phenomenon. This value fits the return intervals that are anticipated for Mediterranean thermophilic forests. By comparison, fire return intervals in modern Mediterranean forests range from 25 to 100 years (Pausas, 2012). Other estimates based on similar methods, such as those from Lake dell'Accesa in Italy (Vannière et al., 2008), indicate that the Holocene's mean fire return interval was approximately 150 years, with a minimum of about 80 years and a maximum of about 450 years. Perhaps the activation of these fires facilitated the replacement of pine forests by thermophilous woodlands as they did during the laurel forest-pine forest boundary in the pre-LGM.

4.4. African Humid Period (AHP, 11.7–5 cal ka BP)

During this period (and the rest of the Holocene) pollen preservation is very poor (samples 160–60 cm). The sole preserved pollen sample at the onset of this period reveals a vegetation composition similar to that

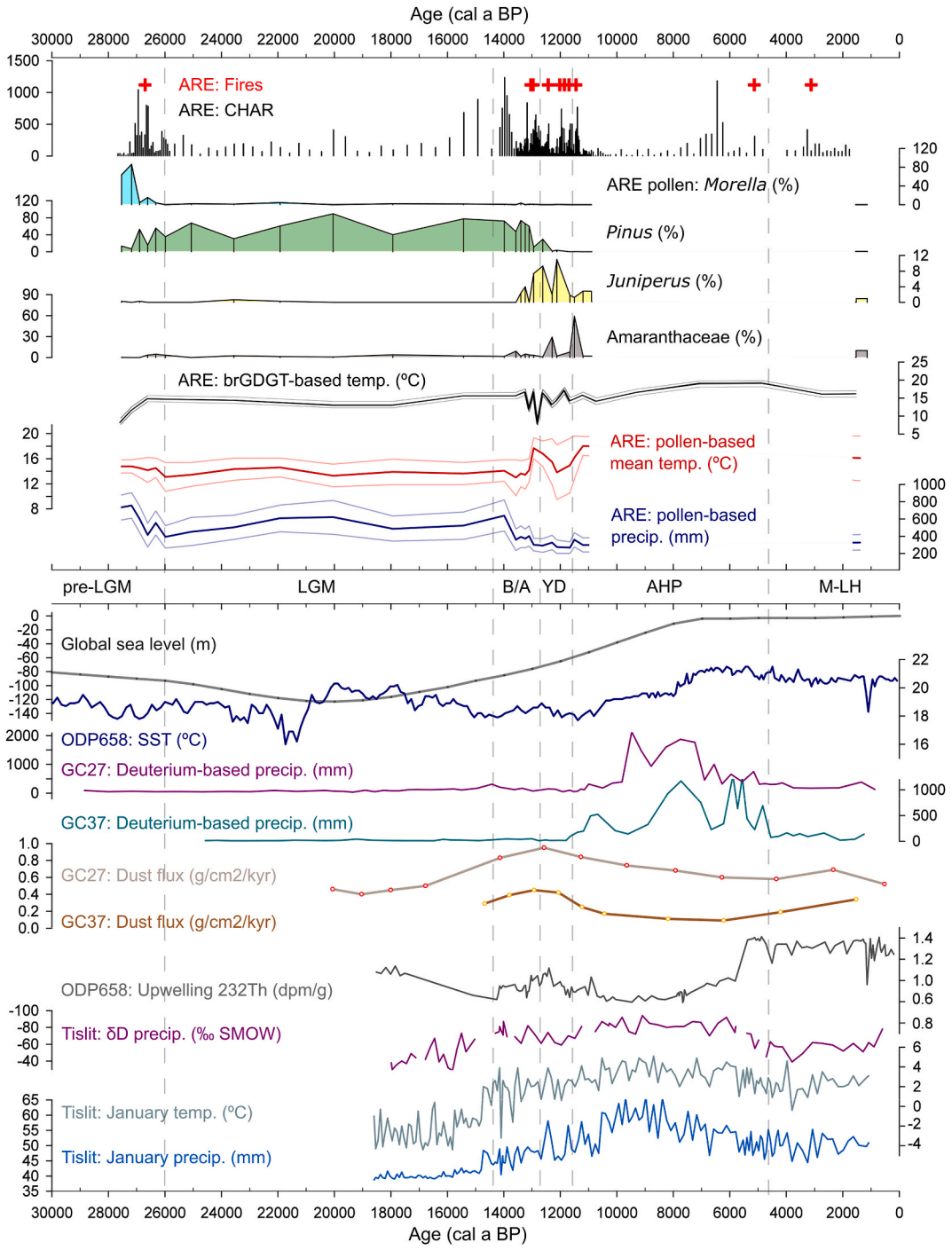

Fig. 6. Multi-proxy diagram of the Vega de Arucas sedimentary sequence (ARE) in Gran Canaria, with selected fire-history data, pollen taxa that best represent shifts in vegetation belts and palaeoclimatic proxies (upper panel). Bottom panel shows curves of sea level, sea surface temperature (SST), and precipitation obtained from marine sedimentary records (ODP658, GC27, GC37). Upwelling and dust input, obtained from marine (ODP658, GC27, GC37) and terrestrial (Tislit) sedimentary records from northwest Africa published in other studies: Global sea level: Cutler et al. (2003), GC27, GC37 dust: Mcgee et al. (2013), GC27, GC37 precipitation: Tierney et al. (2017), ODP658 SST: Zhao et al. (1995), ODP658 232Th: Adkins et al. (2006), Tislit: Cheddadi et al. (2021), pre-LGM: pre-Last Glacial Maximum (30–26 cal ka BP), LGM: Last Glacial Maximum (c. 26–14.5 cal ka BP), B/A: Bølling-Allerød (14.5–12.9 cal ka BP), YD: Younger Dryas (12.9–11.7 cal ka BP), AHP: Early Holocene/African Humid Period (11.7–5 cal ka BP), M-LH: Middle and Late Holocene (5 cal ka BP–present).

of the last deglaciation, characterised by thermophilic species. This suggests that temperatures were higher during this time, a trend further supported by an increase in brGDGT-based temperatures from ~14 to ~19 °C. This is consistent with what is expected for the early Holocene at global scale and the African Humid Period (AHP) regionally, characterised by higher temperatures during the climatic optimum (between ~10,000 and ~6000 cal a BP) due to almost 8 % more summer solar radiation in the Northern Hemisphere than at present (Roberts, 2009).

However, this climatic optimum took different forms: in the tropics and in North Africa, it corresponded to a "pluvial" or humid period that most likely also affected the Canary Islands (Roberts, 2009). North African climate models indicate that the movement of the Intertropical Convergence Zone (ITCZ) is the main cause of humid periods. The ITCZ moved southward as the North Atlantic cooled and northern boreal

insolation decreased, by contrast, the ITCZ shifted to higher latitudes due to increased northern boreal insolation, and precipitation increased throughout most of North Africa (Prell and Kutzbach, 1987; Menviel et al., 2021). This ITCZ shift northward caused the Sahara to become greener during the AHP. Reduced dust in Saharan dunes, reconstructed increases in precipitation based on marine sediments, and vegetation changes in North Africa indicating greening (Kuhlmann et al., 2004; Lézine, 2009; Watrin et al., 2009; Hély and Lézine, 2014) are just a few records that attest to this phenomenon (Fig. 6).

Multiple lines of evidence suggest a period of increased humidity in the Canary Islands coinciding with the AHP. In Gran Canaria, sediment avalanches in Tenteniguada indicate a humid episode that aligns with the onset of the AHP (Lomoschitz et al., 2008). Dune records in Fuerteventura and Lanzarote hold a mix of bioclastic sands and Saharan dust likely deposited during blood rain episodes at the end of the Pleistocene (Criado et al., 2012). Similarly, Damnati et al. (1996) and Coello et al. (1999) identify humid phases around 8–9 ka cal BP.

Possibly, these changes in climate also affected the fire regime. During the AHP, the shortest return interval in the record is observed (102 years, 11,595 cal a BP), although in this period there is also high variability, with some of the longest fire return intervals in the record. One could hypothesise that the fire return interval was shorter with the increase in temperatures during the beginning of the Holocene but its length increased with the arrival of AHP moisture.

Unlike other periods, the Holocene volcanism of Gran Canaria is well-dated (Rodríguez González, 2009), which also allows us to study the relevance of this ignition source. No correlations between volcanic eruptions and fire events were observed, highlighting the fact that the climate plays a major role in determining fire events, in relation to lightning frequency. This conforms with the fire record reconstructed from La Calderilla (Gran Canaria summit, 1770 m a.s.l.) sedimentary sequence (Ravazzi et al., 2021) (Fig. 1).

4.5. Middle and Late Holocene (M-LH, 5–0 cal ka BP)

During the Middle and Late Holocene (M-LH), the poor preservation of pollen in our record hinders the documentation of potential vegetation changes, despite evidence from other studies indicating that regional climatic conditions underwent substantial alterations. The upper 50 cm of the sample, corresponding to ~1140 cal a BP, shows poor preservation but provides evidence suggesting the persistence of thermophilous vegetation during this period. This observation agrees with the palaeoecological record from Laguna de Valleseco (870 m a.s.l.) (Fig. 1), which documents thermophilous woodlands from 4500 to 2300 cal a BP (de Nascimento et al., 2016). Anthracological studies from La Cerera (Fig. 1) further support this, revealing human use of *Juniperus* spp., since at least c. 1600 cal a BP (Becerra Romero et al., 2009). These observations are consistent with the potential vegetation of the area, where Vega de Arucas is classified as a hygrophilous Canary Island palm tree community (del Arco et al., 2006) (Fig. 1). Historical accounts also suggest the presence of a wetland dominated by *Juncus acutus* (Caballero Mujica, 1974).

After the southward shift of the ITCZ to its present-day latitudes, the AHP ended, resulting in the second half of the Holocene being considerably drier than the first. The savannahs and C4 grasslands that covered the Sahara during the AHP moved southwards to their current locations in the Sahel, and the Green Sahara entirely vanished (Kuechler et al., 2013). After this shift, the Canary Current and the strength of the trade winds once again dominated the environment, supporting upwelling and the influx of Saharan dust (Adkins et al., 2006; McGee et al., 2013). Our brGDGT data indicate an average temperature of roughly 17 °C, which falls within the range of the previous period (AHP) and coincides with the estimates from the pollen-based climate model for the upper pollen sample within uncertainties.

Regarding fire records during the M-LH, three fire events with varying return intervals are detected at ARE. In the more recent part of the sequence, we can look for human influence, as detected in other records from the island. Specifically, studies from La Calderilla (4.8–0 cal ka BP) (Ravazzi et al., 2021) and Laguna de Valleseco (4.5–1.5 cal ka BP) (de Nascimento et al., 2016) have shown an increase in charcoal concentration starting around 2 ka, which is interpreted as a result of human activity given its temporal proximity to the settlement of the islands. However, recent revisions to the chronology of human colonisation suggest that the first arrival of humans to Gran Canaria occurred around 1.46–1.42 cal ka BP (Santana et al., 2024). Since our record only extends up to 1.57 cal ka BP, it is possible that it predates the main phase of anthropogenic fire activity on the island. Therefore, the absence of a charcoal peak in Vega de Arucas may reflect this chronological limitation rather than a true absence of human influence. Alternatively, it could also result from agricultural disturbance affecting the upper part of the record or a delayed human impact in this specific region. Lack of palynomorph preservation in these samples prevents us from analysing other anthropogenic landscape modifications on the site.

5. Conclusions

The study of the Vega de Arucas sequence has allowed us to characterise local climatic, vegetation, and fire changes between 27 and 1.5 cal ka BP, as well as vegetation changes from 27 to 11 cal ka BP, most of which correspond to natural variations. Past climate in Gran Canaria does not appear to have been as stable as previously thought. Remarkable climatic variations are detected during the onset of the LGM, deglaciation, and early Holocene, meaning that the Canary Islands vegetation is clearly sensitive to changing climatic conditions, having experienced major transformations over the past 30,000 years. As expected, these natural climatic changes have led to altitudinal shifts in vegetation zones and their associated species. In the Vega de Arucas, the laurel forest was replaced by a pine forest, which was later succeeded by a thermophilous woodland. In addition to changes linked to altitudinal shifts, more subtle changes have also been detected, such as variations in species composition within the same vegetation zone (laurel forest without *Erica*, lack of the representative windward understory in the pine forest).

The fire regime and fire return intervals have also been affected by these climatic changes, influenced no only by a complex combination of these parameters: fires in the Arucas basin were most frequent during transitions between vegetation types (28–26 cal ka BP and 13–11 cal ka BP) but were rare when pine forests dominated (27–13 cal ka BP). This pattern contrasts with modern expectations of higher fire frequency in pine forests, so the decrease in fires after pine forest establishment may be due to the colder, drier conditions prevailing in the LGM. A similar fire-driven transition occurred during the YD, aiding the spread of thermophilous woodlands. During the Holocene, fire frequency varied, with periods of over 1000 years without fires.

Looking at the past provides valuable information on how the Canary Islands responded to climatic conditions that are not analogous to the present, allowing us to outline scenarios of the complex consequences that current and future climatic changes may bring. The use of multiple indicators in the presented climatic reconstructions has allowed us to overcome the limitations of the absence or low detection of some indicators due to post-depositional issues. However, further analysis such as brGDGT local calibration, higher-resolution charcoal studies, phytoliths analysis, sites with complete Holocene pollen records, and more records from different islands, elevations, and exposures will greatly enhance our understanding of past climatic variations in the Canary Islands.

CRediT authorship contribution statement

Pilar Martin-Ramos: Conceptualization, Methodology, Software, Formal analysis, Investigation, Data curation, Writing – original draft, Writing – review & editing, Visualization. **Alvaro Castilla-Beltrán:**

Conceptualization, Methodology, Software, Formal analysis, Investigation, Data curation, Writing – original draft, Writing – review & editing, Visualization, Supervision. **Nina Davtian:** Methodology, Software, Formal analysis, Investigation, Writing – review & editing, Supervision. **José María Fernández-Palacios:** Conceptualization, Investigation, Resources, Writing – original draft, Writing – review & editing, Project administration, Funding acquisition. **Enrique Fernández-Palacios:** Investigation, Writing – original draft, Writing – review & editing. **Agustín Naranjo-Cigala:** Conceptualization, Investigation, Resources, Writing – review & editing, Funding acquisition. **Sandra Nogué:** Conceptualization, Investigation, Writing – review & editing. **Joan Villanueva:** Conceptualization, Methodology, Investigation, Resources, Writing – review & editing, Funding acquisition. **Janet M. Wilmshurst:** Methodology, Formal analysis, Investigation, Resources, Writing – review & editing, Supervision. **Lea de Nascimento:** Conceptualization, Methodology, Formal analysis, Investigation, Resources, Data curation, Investigation, Writing – review & editing, Visualization, Supervision, Project administration, Funding acquisition.

Declaration of Competing interest

We hereby declare that there is no conflict of interest regarding the submission of our paper to Quaternary Science Reviews. All authors have contributed to the research and manuscript preparation, and there are no financial, personal, or professional relationships that could be perceived as a conflict of interest.

Acknowledgements

This research has been framed within the project ISLANDPALECO that has received funding from the European Union's Horizon 2020 research and innovation program under the Marie Skłodowska-Curie grant agreement No 700952 and supported L.d.N. postdoctoral fellowship, and the project "Detección de cambios climáticos del pasado en Canarias", financed by the Consejería de Transición Ecológica, Lucha contra el Cambio Climático y Planificación Territorial, Gobierno de Canarias. S.N. acknowledges support from the European Research Council grant TIME-LINES ERC-CoG-2021 101045309. A.C.B. received funding from the Juan de la Cierva Formación Postdoctoral Research Grant (FJC 2020-043774-I), Ministerio de Ciencia, Innovación y Universidades (Spanish Ministry of Science, Innovation and Universities), and was supported by the Planclimac 2 project (Desarrollo y monitorización de actuaciones coordinadas en la región Macaronesia en materia de riesgos y amenazas del cambio climático (1/MAC/2/April 2, 0006)), co-financed by the European Union Interreg Cooperation Program VI-D MAC (Madeira-Azores-Canarias) 2021–2027. E.F.P. was supported by a Formación de Profesorado Universitario grant (FPU 2019-02379) funded by Ministerio de Ciencia, Innovación y Universidades (Spanish Ministry of Science, Innovation and Universities). We thank Peter Morgan for the sedimentological analyses carried out in the Southampton School of Geography and environmental science. Fundación Arehucas provided permission to work at their property and generously funded the coring for sample collection. We thank Javier Méndez for assistance with sample collection during field work. We thank Constantino Criado Hernández for his thorough review of the manuscript and for providing useful suggestions. We thank the two anonymous reviewers for their useful comments.

Appendix A. Supplementary data

Supplementary data to this article can be found online at https://doi.org/10.1016/j.quascirev.2025.109576.

Data availability

All data and/or code is contained within the submission.

References

Adkins, J., de Menocal, P., Eshel, G., 2006. The "African humid period" and the record of marine upwelling from excess ^{230}Th in Ocean Drilling Program Hole 658C. Paleoceanography 21 (4), PA4203. https://doi.org/10.1029/2005PA001200.

Agencia Estatal de Meteorología (AEMET), 2024. Base de datos climatológica. https://www.aemet.es/es/datos_abiertos/AEMET_OpenData.

Anderson, C.L., Channing, A., Zamuner, A.B., 2009. Life, death and fossilization on Gran Canaria–implications for Macaronesian biogeography and molecular dating. J. Biogeogr. 36 (12), 2189–2201. https://doi.org/10.1111/j.1365-2699.2009.02222.x.

Arévalo, J.R., Bernardos, M., González-Montelongo, C., Grillo, F., 2023. Prescribed burning effect on the richness, diversity and forest structure of an endemic reforested *Pinus canariensis* stand (Canary Islands). Fire 6 (4), 150. https://doi.org/10.3390/fire6040150.

Arévalo, J.R., Fernández-Lugo, S., Naranjo-Cigala, A., Salas, M., Ruíz, R., Ramos, R., Moreno, M., 2014. Post-fire recovery of an endemic Canarian pine forest. Int. J. Wildland Fire 23 (3), 403–409. https://doi.org/10.1071/wf13055.

Arévalo, J.R., Fernández-Palacios, J.M., Jiménez, M.J., Gil, P., 2001. The effect of fire intensity on the understory species composition of two *Pinus canariensis* reforested stands in Tenerife (Canary Islands). For. Ecol. Manag. 148 (1), 21–29. https://doi.org/10.1016/s0378-1127(00)00478-3.

Arévalo, J., Naranjo-Cigala, A., 2018. Wildfire impact and the "fire paradox" in a natural and endemic pine forest stand and shrubland. Fire 1 (3), 44–51. https://doi.org/10.3390/fire1030044.

Banco de Datos de Biodiversidad de Canarias. Gobierno de Canarias. https://www.biodiversidadcanarias.es/biota. (Accessed 1 June 2024).

Bañares, Á., Blanca, G., Güemes, J., Moreno, J.C., Ortiz, S. (Eds.), 2004. Atlas y libro rojo de la flora vascular amenazada de España. Dirección General de Conservación de la Naturaleza, Madrid.

Bartlein, P.J., Harrison, S.P., Brewer, S., Connor, S., Davis, B.A.S., Gajewski, K., Guiot, J., Harrison-Prentice, T.I., Henderson, A., Peyron, O., Prentice, I.C., Scholze, M., Seppä, H., Shuman, B., Sugita, S., Thompson, R.S., Viau, A.E., Williams, J., Wu, H., 2011. Pollen-based continental climate reconstructions at 6 and 21 ka: a global synthesis. Clim. Dyn. 37, 775–802. https://doi.org/10.1007/s00382-010-0904-1.

Becerra Romero, D., Castro-Reino, S.F., Criado Hernández, C., González Quintero, P., Hansen Machín, A., Hernández Padrón, A.J., Jiménez Medina, A.M., Machado Yánez, C., Mendoza Medina, F.A., Mesa Hernández, E.M., Morales Mateo, J., Moreno Benítez, M.A., Rodríguez Rodríguez, A.C., Suárez Medina, I., Tacoronte del Toro, T., Zamora Maldonado, J.M., Correa, T., 2009. El yacimiento arqueológico de La Cerera. Cabildo de Gran Canaria, Consejería de Cultura y Patrimonio Histórico y Cultural. Las Palmas de Gran Canaria.

Bello-Rodríguez, V., Gómez, L.A., Fernández, Á., Del-Arco-Aguilar, M.J., Hernández-Hernández, R., Emerson, B., González-Mancebo, J.M., 2018. Short- and long-term effects of fire in subtropical cloud forests on an oceanic island. Land Degrad. Dev. 30 (4), 448–458. https://doi.org/10.1002/ldr.3237.

Bello-Rodríguez, V., Cubas, J., Del Arco, M.J., Martín, J.L., González-Mancebo, J.M., 2019. Elevational and structural shifts in the treeline of an oceanic island (Tenerife, Canary Islands) in the context of global warming. Int. J. Appl. Earth Obs. Geoinf. 82, 101918. https://doi.org/10.1016/j.jag.2019.101918.

Bennett, K.D., Willis, K.J., 2001. Pollen. Tracking environmental change using lake sediments. In: Smol, J.P., Birks, H.J.B., Last, W.M. (Eds.), Vol. 3: Terrestrial, Algal, and Siliceous Indicators. Kluwer Academic Publishers, Dordrecht, The Netherlands.

Birks, H.H., Birks, H.J.B., 2006. Multi-proxy studies in palaeolimnology. Veg. Hist. Archaeobot. 15, 235–251. https://doi.org/10.1007/s00334-006-0066-6.

Björck, S., Rittenour, T., Rosén, P., França, Z., Möller, P., Snowball, I., Wastegård, S., Bennike, O., Kromer, B., 2006. A Holocene lacustrine record in the central North Atlantic: proxies for volcanic activity, short-term NAO mode variability, and long-term precipitation changes. Quat. Sci. Rev. 25 (1–2), 9–32. https://doi.org/10.1016/j.quascirev.2005.08.008.

Blaauw, M., Christen, J.A., 2013. Bacon Manual v2.3.3.

Bowen, D.Q., 2009. Last glacial maximum. In: Encyclopedia of Paleoclimatology and Ancient Environments. Encyclopedia of Earth Sciences Series. Springer, Dordrecht. https://doi.org/10.1007/978-1-4020-4411-3_122.

Brunelle, A., Minckley, T.A., Shinker, J.J., Heyer, J., 2018. Filling a geographical gap: new palaeoecological reconstructions from the Desert Southwest, USA. Front. Earth Sci. 6. https://doi.org/10.3389/feart.2018.00106.

Caballero Mujica, F., 1974. Pedro Cerón y el Mayorazgo de Arucas. Ayuntamiento de Arucas. Las Palmas de Gran Canaria.

Caromano, C.F., Cascon, L.M., 2014. Charcoal: preservation and conservation. In: Smith, C. (Ed.), Encyclopedia of Global Archaeology. Springer, New York. https://doi.org/10.1007/978-1-4419-0465-2_481.

Castilla-Beltrán, A., de Lima, R.F., Bosco, L.B., Armas, R.D.C., Strandberg, N., Stévart, T., de Nascimento, L., Fernández-Palacios, J.M., Nogué, S., 2023. 14,000 years of climatic and anthropogenic change in the Afromontane forest of São Tomé Island, Gulf of Guinea. Quat. Sci. Rev. 322, 108381. https://doi.org/10.1016/j.quascirev.2023.108381.

Cheddadi, R., Carré, M., Nourelbait, M., François, L., Rhoujjati, A., Manay, R., Schefuß, E., 2021. Early Holocene greening of the Sahara requires Mediterranean winter rainfall. Proc. Natl. Acad. Sci. U.S.A. 118 (23), e2024898118.

Chen, Y., Zheng, F., Yang, H., Yang, W., Wu, R., Liu, X., Liang, H., Chen, H., Pei, H., Zhang, C., Pancost, R.D., Zeng, Z., 2022. The production of diverse brGDGTs by an Acidobacterium providing a physiological basis for paleoclimate proxies. Geochem. Cosmochim. Acta 337, 155–165. https://doi.org/10.1016/j.gca.2022.08.033.

Chevalier, M., Cheddadi, R., Chase, B.M., 2014. CREST: climate REconstruction SofTware. Clim. Past 10, 625–663. https://doi.org/10.5194/cp-10-2081-2014.

Chevalier, M., Davis, B.A., Heiri, O., Seppä, H., Chase, B.M., Gajewski, K., Lacourse, T., Telford, R.J., Finsinger, W., Guiot, J., Kühl, N., Maezumi, S.Y., Tipton, J.R., Carter, V.A., Brussel, T., Phelps, L.N., Dawson, A., Zanon, M., Vallé, F., Nolan, C., Kupriyanov, D., 2020. Pollen-based climate reconstruction techniques for late Quaternary studies. Earth Sci. Rev. 210, 103384. https://doi.org/10.1016/j.earscirev.2020.103384.

Clark, P.U., Mix, A.C., 2002. Ice sheets and sea level of the Last Glacial Maximum. Quat. Sci. Rev. 21 (1–3), 1–7. https://doi.org/10.1016/S0277-3791(01)00118-4.

Climent, J., Tapias, R., Pardos, J.A., Gil, L., 2004. Fire adaptations in the Canary Islands pine *(Pinus canariensis)*. Plant Ecol. 171 (1), 185–196. https://doi.org/10.1023/b:vege.0000029374.64778.68.

Coello, J.J., Castillo, C., González, E.M., 1999. Stratigraphy, chronology, and paleoenvironmental reconstruction of the Quaternary sedimentary infilling of a volcanic tube in Fuerteventura, Canary Islands. Quat. Res. 52 (3), 360–368. https://doi.org/10.1006/qres.1999.2074.

Collins, J.A., Govin, A., Mulitza, S., Heslop, D., Zabel, M., Hartmann, J., Röhl, U., Wefer, G., 2013. Abrupt shifts of the Sahara–Sahel boundary during Heinrich stadials. Clim. Past 9, 1181–1191. https://doi.org/10.5194/cp-9-1181-2013.

Conedera, M., Tinner, W., Neff, C., Meurer, M., Dickens, A.F., Krebs, P., 2009. Reconstructing past fire regimes: methods, applications, and relevance to fire management and conservation. Quat. Sci. Rev. 28 (5), 555–576. https://doi.org/10.1016/j.quascirev.2008.11.005.

Crausbay, S., Genderjahn, S., Hotchkiss, S., Sachse, D., Kahmen, A., Arndt, S.K., 2014. Vegetation dynamics at the upper reaches of a tropical montane forest are driven by disturbance over the past 7300 years. Arctic Antarct. Alpine Res. 46 (4), 787–799. https://doi.org/10.1657/1938-4246-46.4.787.

Crema, E., Bevan, A., 2021. Inference from large sets of radiocarbon dates: software and methods. Radiocarbon 63, 23–39. https://doi.org/10.1017/RDC.2020.95.

Criado, C., Dorta, P., 2003. An unusual 'blood rain' over the Canary Islands (Spain). The storm of January 1999. J. Arid Environ. 55 (4), 765–783. https://doi.org/10.1016/S0140-1963(02)00320-8.

Criado, C., Torres, J.M., Hansen, A.R., Lillo, P., Naranjo, A., 2012. Intercalaciones de polvo sahariano en paleodunas bioclásticas de Fuerteventura (Islas Canarias. Cuaternario Geomorfol. 26 (1-2), 73–88.

Croudace, I.W., Rothwell, R.G. (Eds.), 2015. *Micro-XRF Studies of Sediment Cores: Applications of a non-destructive tool for the environmental*. sciences, 17. Springer, Dordrecht.

Cutler, K.B., Edwards, R.L., Taylor, F.W., Cheng, H., Adkins, J., Gallup, C.D., Bloom, A.L., 2003. Rapid sea-level fall and deep-ocean temperature change since the last interglacial period. Earth Planet. Sci. Lett. 206 (3–4), 253–271. https://doi.org/10.1016/S0012-821X(02)01107-X.

Damnati, B., Petit-Maire, N., Fontugne, M., Meco, J., Williamson, D., 1996. Quaternary palaeoclimates in the eastern Canary Islands. Quat. Int. 31, 37–46. https://doi.org/10.1016/1040-6182(95)00019-F.

Dang, X., Yang, H., Naafs, B.D.A., Pancost, R.D., Xie, S., 2016. Evidence of moisture control on the methylation of branched glycerol dialkyl glycerol tetraethers in semi-arid and arid soils. Geochem. Cosmochim. Acta 189, 24–36. https://doi.org/10.1016/j.gca.2016.06.004.

Davtian, N., Ménot, G., Bard, E., Poulenard, J., Podwojewski, P., 2016. Consideration of soil types for the calibration of molecular proxies for soil pH and temperature using global soil datasets and Vietnamese soil profiles. Org. Geochem. 101, 140–153. https://doi.org/10.1016/j.orggeochem.2016.09.002.

Davtian, N., Ménot, G., Fagault, Y., Bard, E., 2019. Western Mediterranean Sea paleothermometry over the last glacial cycle based on the novel RI-OH Index. Paleoceanogr. Paleoclimatol. 34 (4), 616–634. https://doi.org/10.1029/2018PA003452.

de Boer, E.J., Hooghiemstra, H., Vincent Florens, F.B., Baider, C., Engels, S., Dakos, V., Blaauw, M., Bennett, K.D., 2013. Rapid succession of plant associations on the small ocean island of Mauritius at the onset of the Holocene. Quat. Sci. Rev. 68, 114–125. https://doi.org/10.1016/j.quascirev.2013.02.005.

De Jonge, C., Hopmans, E.C., Stadnitskaia, A., Rijpstra, W.I.C., Hofland, R., Tegelaar, E., Sinninghe Damsté, J.S., 2013. Identification of novel penta- and hexamethylated branched glycerol dialkyl glycerol tetraethers in peat using HPLC–MS^2, GC–MS and GC–SMB-MS. Org. Geochem. 54, 78–82. https://doi.org/10.1016/j.orggeochem.2012.10.004.

De Jonge, C., Hopmans, E.C., Zell, C.I., Kim, J.H., Schouten, S., Sinninghe Damsté, J.S., 2014. Occurrence and abundance of 6-methyl branched glycerol dialkyl glycerol tetraethers in soils: implications for palaeoclimate reconstruction. Geochem. Cosmochim. Acta 141, 97–112. https://doi.org/10.1016/j.gca.2014.06.013.

De Jonge, C., Peterse, F., Nierop, K.G., Blattmann, T.M., Alexandre, M., Ansanay-Alex, S., Austin, T., Babin, M., Bard, E., Bauersachs, T., Blewett, J., Boehman, B., Castañeda, I. S., Chen, J., Conti, M.L.G., Contreras, S., Cordes, J., Davtian, N., van Dongen, B., et al., 2024a. Interlaboratory comparison of branched GDGT temperature and pH proxies using soils and lipid extracts. G-cubed 25 (7), e2024GC011583. https://doi.org/10.1029/2024GC011583.

De Jonge, C., Guo, J., Hällberg, P., Griepentrog, M., Rifai, H., Richter, A., Ramirez, E., Zhang, X., Smittenberg, R.H., Peterse, F., Boeckx, P., Dercon, G., 2024b. The impact of soil chemistry, moisture and temperature on branched and isoprenoid GDGTs in soils: a study using six globally distributed elevation transects. Org. Geochem. 187, 104706. https://doi.org/10.1016/j.orggeochem.2023.104706.

de Nascimento, L., Willis, K.J., Fernández-Palacios, J.M., Criado, C., Whittaker, R.J., 2009. The long-term ecology of the lost forests of La Laguna, Tenerife (Canary Islands). J. Biogeogr. 36 (3), 499–514. https://doi.org/10.1111/j.1365-2699.2008.02012.x.

de Nascimento, L., Nogué, S., Fernández-Lugo, S., Méndez, J., Otto, R., Whittaker, R.J., Willis, K.J., Fernández-Palacios, J.M., 2015. Modern pollen rain in Canary Island ecosystems and its implications for the interpretation of fossil records. Rev. Palaeobot. Palynol. 214, 27–39. https://doi.org/10.1016/j.revpalbo.2014.11.002.

de Nascimento, L., Nogué, S., Criado, C., Ravazzi, C., Whittaker, R.J., Willis, K.J., Fernández-Palacios, J.M., 2016. Reconstructing Holocene vegetation on the island of Gran Canaria before and after human colonisation. Holocene 26 (1), 113–125. https://doi.org/10.1177/0959683615596836.

del Arco, M.J., Rodríguez Delgado, O., 2018. Vegetation of the Canary Islands. Springer International Publishing, Cham, Switzerland. https://doi.org/10.1007/978-3-319-77255-4.

del Arco, M.J., Wildpret, W., Pérez de Paz, P.L., Rodríguez, O., Acebes, J.R., García, A., Martín, V.E., Reyes, J.A., Salas, M., Díaz, M.A., Bermejo, J.A., González, R., Cabrera, M.V., García, S., 2006. Mapa de vegetación de Canarias. GRAFCAN, Santa Cruz de Tenerife.

Dearing Crampton-Flood, E., Tierney, J.E., Peterse, F., Kirkels, F.M.S.A., Sinninghe Damsté, J.S., 2020. BayMBT: a Bayesian calibration model for branched glycerol dialkyl glycerol tetraethers in soils and peats. Geochem. Cosmochim. Acta 268, 142–159. https://doi.org/10.1016/j.gca.2019.09.043.

Díaz Elías, M.B., 2014. Plan General de Ordenación Arucas. Volumen 6. Documentación ambiental del plan de junio 2014. Comisión de Ordenación del Territorio y Medio Ambiente de Canarias, Las Palmas de Gran Canaria, Spain. http://www.idecanarias.es/resources/PLA_ENP_URB/URB_PLA/GC/Aruc/759/TIP/pgo_aruc_isa01.pdf.

Díaz Fernández, R.F., 1989. Breve síntesis de la historia de Arucas. Aguayro 181, 16–18.

Ding, S., Schwab, V.F., Ueberschaar, N., Roth, V.-N., Lange, M., Xu, Y., Gleixner, G., Pohnert, G., 2016. Identification of novel 7-methyl and cyclopentanyl branched glycerol dialkyl glycerol tetraethers in lake sediments. Org. Geochem. 102, 52–58. https://doi.org/10.1016/j.orggeochem.2016.09.009.

Dirghangi, S.S., Pagani, M., Hren, M.T., Tipple, B.J., 2013. Distribution of glycerol dialkyl glycerol tetraethers in soils from two environmental transects in the USA. Org. Geochem. 59, 49–60. https://doi.org/10.1016/j.orggeochem.2013.03.009.

Duan, Y., Sun, Q., Werne, J.P., Yang, H., Jia, J., Wang, L., Xie, H., Chen, F., 2020. Soil pH dominates the distributions of both 5- and 6-methyl branched tetraethers in arid regions. J. Geophys. Res.: Biogeosciences 125 (10), e2019JG005356. https://doi.org/10.1029/2019JG005356.

Duan, Y., Sun, Q., Werne, J.P., Hou, J., Yang, H., Wang, Q., Khormali, F., Chen, F., 2022. The impact of precipitation on the distributions of branched tetraethers in alkaline soils. Org. Geochem. 169, 104410. https://doi.org/10.1016/j.orggeochem.2022.104410.

Fernández-Palacios, J.M., Arévalo, J.R., Balguerías, E., Barone, R., de Nascimento, L., Elias, R.B., et al., 2017. *La Laurisilva. Canarias, Madeira y Azores.* Macaronesia Editorial. Santa Cruz de Tenerife, Spain.

Fernández-Palacios, J.M., Kreft, H., Irl, S.D.H., Norder, S., Ah-Peng, C., Borges, P.A.V., Burns, K.C., de Nascimento, L., Meyer, J.-Y., Montes, E., Drake, D.R., 2021. Scientists' warning: the outstanding biodiversity of islands is in peril. Glob. Ecol. Conserv. 31, e01847. https://doi.org/10.1016/j.gecco.2021.e01847.

Fernández-Palacios, J.M., Arévalo, J.R., Barone, R., Castilla-Beltrán, A., de Nascimento, L., Duarte, M., Fernández-Palacios, E., Naranjo-Cigala, A., Nogué, S., Otto, R., Romeiras, M., Sierra Cornejo, N., 2024. Los Bosques Termófilos: Canarias, Madeira y Cabo Verde. Macaronesia Editorial, Santa Cruz de Tenerife, Spain.

Fernández-Palacios, J.M., Rijsdijk, K.F., Norder, S.J., Otto, R., de Nascimento, L., Fernández-Lugo, S., Whittaker, R.J., 2016. Towards a glacial-sensitive model of island biogeography. Glob. Ecol. Biogeogr. Global Ecology and Biogeography 25 (7), 817–830. https://doi.org/10.1111/geb.12320.

Feurdean, A., Florescu, G., Tanţău, I., Vannière, B., Diaconu, A.C., Pfeiffer, M., Warren, D., Hutchinson, S.M., Gorina, N., Gałka, M., Kirpotin, S., 2020. Recent fire regime in the southern boreal forests of western Siberia is unprecedented in the last five millennia. Quat. Sci. Rev. 244, 106495. https://doi.org/10.1016/j.quascirev.2020.106495.

Finsinger, W., Bonnici, I.. - tapas: an R package to perform trend and peaks analysis. https://doi.org/10.5281/zenodo.6344463.

Finsinger, W., Tinner, W., 2005. Minimum count sums for charcoal concentration estimates in pollen slides: accuracy and potential errors. Holocene 15 (2), 293–297. https://doi.org/10.1191/0959683605hl808rr.

García-López, M.A., Rozas, V., Olano, J.M., Sangüesa-Barreda, G., García-Hidalgo, M., Gómez-González, S., López-Rubio, R., Fernández-Palacios, J.M., García-González, I., García-Cervigón, A.I., 2022. Tree-ring distinctness, dating potential and climatic sensitivity of laurel forest tree species in Tenerife Island. Dendrochronologia 76, 126011. https://doi.org/10.1016/j.dendro.2022.126011.

Garzón-Machado, V., del Arco, M.J., González, F.V., Pérez-de-Paz, P.L., 2012. Fire as a threatening factor for endemic plants of the Canary Islands. Biodivers. Conserv. 21, 2621–2632. https://doi.org/10.1007/s10531-012-0321-3.

Gilman, S.E., Urban, M.C., Tewksbury, J., Gilchrist, G.W., Holt, R.D., 2010. A framework for community interactions under climate change. Trends Ecol. Evol. 25 (6), 325–331. https://doi.org/10.1016/j.tree.2010.03.002.

GRAFCAN, 2004. Mapa topográfico 1:20.000. Años 2004-2006. https://idecan1.grafcan.es/ServicioWMS/MT20?service=wms&request=getcapabilities.

Grimm, E., 1993. TILIA: A Pollen Program for Analysis and Display. Illinois State Museum, Springfield.

Guo, J., Ma, T., Liu, N., Zhang, X., Hu, H., Ma, W., Wang, Z., Feng, X., Peterse, F., 2022. Soil pH and aridity influence distributions of branched tetraether lipids in grassland soils along an aridity transect. Org. Geochem. 164, 104347. https://doi.org/10.1016/j.orggeochem.2021.104347.

Guo, J., Ziegler, M., Wanders, N., Vreeken, M., Yin, Q., Lu, H., Fuchs, L., Dong, J., Sun, Y., Peterse, F., 2024. Robust land surface temperature record for north China over the past 21,000 years. Sci. Adv. 10 (8), eadj4800. https://doi.org/10.1126/sciadv.adj4800.

Guo, J., Fuchs, L., Ziegler, M., Sun, Y., Peterse, F., 2025. Assessing tetraether lipids as a paleotemperature proxy on western edge of the Chinese Loess Plateau: a cautionary tale. Org. Geochem. 201, 104947. https://doi.org/10.1016/j.orggeochem.2025.104947.

Häggi, C., Naafs, B.D.A., Silvestro, D., Bertassoli, D.J., Akabane, T.K., Mendes, V.R., Sawakuchi, A.O., Chiessi, C.M., Jaramillo, C.A., Feakins, S.J., 2023. GDGT distribution in tropical soils and its potential as a terrestrial paleothermometer revealed by Bayesian deep-learning models. Geochem. Cosmochim. Acta 362, 41–64. https://doi.org/10.1016/j.gca.2023.09.014.

Halamka, T.A., Raberg, J.H., McFarlin, J.M., Younkin, A.D., Mulligan, C., Liu, X.-L., Kopf, S.H., 2023. Production of diverse brGDGTs by Acidobacterium *Solibacter usitatus* in response to temperature, pH, and O_2 provides a culturing perspective on brGDGT proxies and biosynthesis. Geobiology 21 (1), 102–118. https://doi.org/10.1111/gbi.12525.

Harter, D.E.V., Irl, S.D.H., Seo, B., Steinbauer, M.J., Gillespie, R., Triantis, K.A., Fernández-Palacios, J.M., Beierkuhnlein, C., 2015. Impacts of global climate change on the floras of oceanic islands: Projections, implications, and current knowledge. Perspect. Plant Ecol. Evol. Systemat. 17 (2), 160–183. https://doi.org/10.1016/j.ppees.2015.01.003.

Havinga, A.J., 1967. Palynology and pollen preservation. Rev. Palaeobot. Palynol. 2 (1–4), 81–98.

Heinrich, H., Schmidt, C., Ziemen, F., Mikolajewicz, U., Roettig, C.-B., 2021. Massive deposition of Sahelian dust on the canary island Lanzarote during North Atlantic Heinrich events. Quat. Res. 101, 51–66. https://doi.org/10.1017/qua.2020.100.

Heiri, O., Lotter, A.F., Lemcke, G., 2001. Loss on ignition as a method for estimating organic and carbonate content in sediments: reproducibility and comparability of results. J. Paleolimnol. 25 (1), 101–110. https://doi.org/10.1023/A:1008119611481.

Hély, C., Lézine, A.M., 2014. Holocene changes in African vegetation: Tradeoff between climate and water availability. Clim. Past 10 (2), 681–686. https://doi.org/10.5194/cp-10-681-2014.

Higuera, P., 2009. CharAnalysis 0.9: Diagnostic and analytical tools for sediment-charcoal analysis. User's Guide. Montana State University, Bozeman.

Higuera, P.E., Gavin, D.G., Bartlein, P.J., Hallett, D.J., 2010. Peak detection in sediment-charcoal records: impacts of alternative data analysis methods on fire-history interpretations. Int. J. Wildland Fire 19 (8), 996–1014. https://doi.org/10.1071/WF09134.

Hooghiemstra, H., Lézine, A.-M., Leroy, S.A.G., Dupont, L., Marret, F., 2006. Late Quaternary palynology in marine sediments: a synthesis of the understanding of pollen distribution patterns in the NW African setting. Quat. Int. 148 (1), 29–44. https://doi.org/10.1016/j.quaint.2005.11.005.

Hopmans, E.C., Schouten, S., Sinninghe Damsté, J.S., 2016. The effect of improved chromatography on GDGT-based palaeoproxies. Org. Geochem. 93, 1–6. https://doi.org/10.1016/j.orggeochem.2015.12.006.

Inglis, G.N., Bhattacharya, T., Hemingway, J.D., Hollingsworth, E.H., Feakins, S.J., Tierney, J.E., 2022. Biomarker approaches for reconstructing terrestrial environmental change. Annu. Rev. Earth Planet Sci. 50 (1), 369–394. https://doi.org/10.1146/annurev-earth-032320-095943.

Jansen, E., Overpeck, J., Briffa, K.R., Duplessy, J.-C., Joos, F., Masson-Delmotte, V., Olago, D., Otto-Bliesner, B., Peltier, W.R., Rahmstorf, S., Ramesh, R., Raynaud, D., Rind, D., Solomina, O., Villalba, R., Zhang, D., 2007. Palaeoclimate. In: Solomon, S., Qin, D., Manning, M., Chen, Z., Marquis, M., Averyt, K.B., Tignor, M., Miller, H.L. (Eds.), Climate change 2007: The physical science basis. Contribution of Working Group I to the Fourth Assessment Report of the Intergovernmental Panel on Climate Change. Cambridge University Press, Cambridge, United Kingdom; New York, NY, United States, pp. 1–88.

Jiménez Medina, A.M., 1994. Informe preliminar de las principales áreas arqueológicas del municipio de Arucas (Gran Canaria). In: Pérez-Chacón Espino, E. (Ed.), Estudio detallado de impacto ecológico del plan general de ordenación urbana del municipio de Arucas. Ayuntamiento de Arucas, Arucas.

Kelly, R.F., Higuera, P.E., Barrett, C.M., Hu, F.S., 2011. Short paper: a signal-to-noise index to quantify the potential for peak detection in sediment-charcoal records. Quat. Res. 75 (1), 11–17. https://doi.org/10.1016/j.yqres.2010.07.011.

Kuechler, R.R., Schefuß, E., Beckmann, B., Dupont, L., Wefer, G., 2013. NW African hydrology and vegetation during the Last Glacial Cycle, reflected in plant-wax-specific hydrogen and carbon isotopes. Quat. Sci. Rev. 82, 56–67. https://doi.org/10.1016/j.quascirev.2013.10.013.

Kuhlmann, H., Meggers, H., Freudenthal, T., Wefer, G., 2004. The transition of the monsoonal and the N Atlantic climate system of NW Africa during the Holocene. Geophys. Res. Lett. 31 (22). https://doi.org/10.1029/2004GL021267.

Lembrechts, J.J., van den Hoogen, J., Aalto, J., Ashcroft, M.B., De Frenne, P., Kemppinen, J., Kopecký, M., Luoto, M., Maclean, I.M.D., Crowther, T.W., Bailey, J. J., Haesen, S., Klinges, D.H., Niittynen, P., Scheffers, B.R., Van Meerbeek, K., Aartsma, P., Abdalaze, O., Abedi, M., et al., 2022. Global maps of soil temperature. Glob. Change Biol. 28 (9), 3110–3144. https://doi.org/10.1111/gcb.16060.

Lestienne, M., Jouffroy-Bapicot, I., Leyssenne, D., Sabatier, P., Debret, M., Albertini, P.-J., Colombaroli, D., Didier, J., Hély, C., Vannière, B., 2019. Fires and human activities as key factors in the high diversity of Corsican vegetation. Holocene 30 (2), 244–257. https://doi.org/10.1177/0959683619883025.

Leys, B., Finsinger, W., Carcaillet, C., 2014. Historical range of fire frequency is not the Achilles' heel of the Corsican black pine ecosystem. J. Ecol. 102 (2), 381–395. https://doi.org/10.1111/1365-2745.12207.

Lézine, A.M., 2009. Timing of vegetation changes at the end of the Holocene Humid Period in desert areas at the northern edge of the Atlantic and Indian monsoon systems. C. R. Geosci. 341 (8–9), 750–759. https://doi.org/10.1016/j.crte.2009.01.001.

Liang, J., Russell, J.M., Xie, H., Lupien, R.L., Si, G., Wang, J., Hou, J., Zhang, G., 2019. Vegetation effects on temperature calibrations of branched glycerol dialkyl glycerol tetraether (brGDGTs) in soils. Org. Geochem. 127, 1–11. https://doi.org/10.1016/j.orggeochem.2018.10.010.

Liang, J., Richter, N., Xie, H., Zhao, B., Si, G., Wang, J., Hou, J., Zhang, G., Russell, J.M., 2023. Branched glycerol dialkyl glycerol tetraether (brGDGT) distributions influenced by bacterial community composition in various vegetation soils on the Tibetan Plateau. Palaeogeogr. Palaeoclimatol. Palaeoecol. 611, 111358. https://doi.org/10.1016/j.palaeo.2022.111358.

Lietz, J., Schmincke, H.-U., 1975. Miocene—Pliocene sea-level changes and volcanic phases on Gran Canaria (Canary Islands) in the light of new K—Ar ages. Palaeogeogr. Palaeoclimatol. Palaeoecol. 18 (3), 213–239. https://doi.org/10.1016/0031-0182(75)90034-6.

Ljung, K., Björck, S., 2007. Holocene climate and vegetation dynamics on Nightingale Island, South Atlantic—an apparent interglacial bipolar seesaw in action? Quat. Sci. Rev. 26 (25–28), 3150–3166. https://doi.org/10.1016/j.quascirev.2007.08.003.

Lomoschitz, A., Hervás, J., Yepes, J., 2008. Characterisation of a Pleistocene debris-avalanche deposit in the Tenteniguada basin, Gran Canaria island, Spain. Landslides 5, 227–234. https://doi.org/10.1007/s10346-008-0115-6.

Lu, H., Liu, W., Yang, H., Wang, H., Liu, Z., Leng, Q., Sun, Y., Zhou, W., An, Z., 2019. 800-kyr land temperature variations modulated by vegetation changes on Chinese Loess Plateau. Nat. Commun. 10, 1958. https://doi.org/10.1038/s41467-019-09978-1.

Luque Söllheim, Á.L., Máyer Suarez, P., García Hernández, F., 2024. The digital climate atlas of the Canary Islands: a tool to improve knowledge of climate and temperature and precipitation trends in the Atlantic islands. Clim. Serv. 34, 100487. https://doi.org/10.1016/j.cliser.2024.100487.

McClymont, E.L., Mackay, H., Stevenson, M.A., Damm-Johnsen, T., Honan, E.M., Penny, C.E., Cole, Y.A., 2023. Biomarker proxies for reconstructing Quaternary climate and environmental change. J. Quat. Sci. 38 (7), 991–1024. https://doi.org/10.1002/jqs.3559.

McGee, D., deMenocal, P.B., Winckler, G., Stuut, J.B.W., Bradtmiller, L.I., 2013. magnitude, timing and abruptness of changes in North African dust deposition over the last 20,000 yr. Earth Planet Sci. Lett. 371–372, 163–176. https://doi.org/10.1016/j.epsl.2013.03.054.

McWethy, D.B., Whitlock, C., Wilmshurst, J.M., McGlone, M.S., Fromont, M., Li, X., Dieffenbacher-Krall, A., Hobbs, W.O., Fritz, S.C., Cook, E.R., 2010. Rapid landscape transformation in South Island, New Zealand, following initial Polynesian settlement. Proc. Natl. Acad. Sci. 107 (50), 21343–21348. https://doi.org/10.1073/pnas.1011801107.

McWethy, D.B., Wilmshurst, J.M., Whitlock, C., Wood, J.R., McGlone, M.S., 2014. A high-resolution chronology of rapid forest transitions following Polynesian arrival in New Zealand. PLoS One 9 (11), e111328. https://doi.org/10.1371/journal.pone.0111328.

Martín-Esquivel, J.L., Marrero-Gómez, M., Cubas, J., González-Mancebo, J.M., Olano, J. M., del Arco, M., 2020. Climate warming and introduced herbivores disrupt alpine plant community of an oceanic island (Tenerife, Canary Islands). Plant Ecol. 221, 1117–1131. https://doi.org/10.1007/s11258-020-01066-5.

Martínez-Sosa, P., Tierney, J.E., Stefanescu, I.C., Dearing Crampton-Flood, E., Shuman, B.N., Routson, C., 2021. A global Bayesian temperature calibration for lacustrine brGDGTs. Geochem. Cosmochim. Acta 305, 87–105. https://doi.org/10.1016/j.gca.2021.04.038.

Martínez-Sosa, P., Tierney, J.E., Pérez-Angel, L.C., Stefanescu, I.C., Guo, J., Kirkels, F., Sepúlveda, J., Peterse, F., Shuman, B.N., Reyes, A.V., 2023. Development and application of the Branched and Isoprenoid GDGT Machine learning Classification algorithm (BIGMaC) for paleoenvironmental reconstruction. Paleoceanogr. Paleoclimatol. 38, e2023PA004611. https://doi.org/10.1029/2023PA004611.

Marzol Jaén, M.V., Máyer Suárez, P., 2012. Algunas reflexiones acerca del clima de las Islas Canarias. Nimbus: Revista de climatología, meteorología y paisaje 399–416 (29–30).

Mazei, Y.A., Tsyganov, A.N., Bobrovsky, M.V., Mazei, N.G., Kupriyanov, D.A., Gałka, M., Rostanets, D.V., Khazanova, K.P., Stoiko, T.G., Pastukhova, Y.A., Fatynina, Y.A., Komarov, A.A., Babeshko, K.V., Makarova, A.D., Saldaev, D.A., Zazovskaya, E.P., Dobrovolskaya, M.V., Tiunov, A.V., 2020. Peatland development, vegetation history, climate change and human activity in the Valdai uplands (Central European Russia) during the Holocene: a multi-proxy palaeoecological study. Diversity 12 (12), 462. https://doi.org/10.3390/d12120462.

Medina, A.M.J., 2004. La Laguna de Arucas (Gran Canaria): algunas consideraciones geográficas e históricas. Coloquios de Historia Canario Americana, pp. 49–65.

Menges, J., Huguet, C., Alcañiz, J.M., Fietz, S., Sachse, D., Rosell-Melé, A., 2014. Influence of water availability in the distributions of branched glycerol dialkyl glycerol tetraether in soils of the Iberian Peninsula. Biogeosciences 11, 2571–2581. https://doi.org/10.5194/bg-11-2571-2014.

Méndez, J., Morales, G., de Nascimento, L., Otto, R., Gallardo, A., Fernández-Palacios, J. M., 2015. Understanding long-term post-fire regeneration of a fire-resistant pine species. Ann. For. Sci. 72, 609–619. https://doi.org/10.1007/s13595-015-0482-9.

Menviel, L., Govin, A., Avenas, A., Meissner, K.J., Grant, K.M., Tzedakis, P.C., 2021. Drivers of the evolution and amplitude of African humid periods. Commun. Earth Environ. 2, 237. https://doi.org/10.1038/s43247-021-00309-1.

Molnar, P., 2022. Differences between soil and air temperatures: implications for geological reconstructions of past climate. Geosphere 18 (2), 800–824. https://doi.org/10.1130/GES02448.1.

Moreno, A., Nave, S., Kuhlmann, H., Canals, M., Targarona, J., Freudenthal, T., Abrantes, F., 2002. Productivity response in the North Canary Basin to climate changes during the last 250000 yr: a multi-proxy approach. Earth Planet Sci. Lett. 196, 147–159. https://doi.org/10.1016/S0012-821X(01)00605-7.

Naafs, B.D.A., Gallego-Sala, A.V., Inglis, G.N., Pancost, R.D., 2017a. Refining the global branched glycerol dialkyl glycerol tetraether (brGDGT) soil temperature calibration. Org. Geochem. 106, 48–56. https://doi.org/10.1016/j.orggeochem.2017.01.009.

Naafs, B.D.A., Inglis, G.N., Zheng, Y., Amesbury, M.J., Biester, H., Bindler, R., Blewett, J., Burrows, M.A., del Castillo Torres, D., Chambers, F.M., Cohen, A.D., Evershed, R.P., Feakins, S.J., Gałka, M., Gallego-Sala, A., Gandois, L., Gray, D.M., Hatcher, P.G., Honorio Coronado, E.N., Hughes, P.D.M., Huguet, A., Könönen, M., Laggoun-Défarge, F., Lähteenoja, O., Lamentowicz, M., Marchant, R., McClymont, E., Pontevedra-Pombal, X., Ponton, C., Pourmand, A., Rizzuti, A.M., Rochefort, L., Schellekens, J., De Vleeschouwer, F., Pancost, R.D., 2017b. Introducing global peat-specific temperature and pH calibrations based on brGDGT bacterial lipids. Geochem. Cosmochim. Acta 208, 285–301. https://doi.org/10.1016/j.gca.2017.01.038.

Naafs, B.D.A., Oliveira, A.S.F., Mulholland, A.J., 2021. Molecular dynamics simulations support the hypothesis that the brGDGT paleothermometer is based on homeoviscous adaptation. Geochem. Cosmochim. Acta 312, 44–56. https://doi.org/10.1016/j.gca.2021.07.034.

Navarro-Cerrillo, R.M., Padrón Cedrés, E., Cachinero-Vivar, A.M., Valeriano, C., Camarero, J.J., 2024. Integrating dendrochronological and LiDAR data to improve management of *Pinus canariensis* forests under different thinning and climatic scenarios. Remote Sens. 16, 850. https://doi.org/10.3390/rs16050850.

Ne'eman, G., Arianoutsou, M., 2021. Mediterranean pines – adaptations to fire. In: Ne'eman, G., Osem, Y. (Eds.), Pines and Their Mixed Forest Ecosystems in the Mediterranean Basin, vol. 38. Springer, Cham, Switzerland, pp. 357–373. https://doi.org/10.1007/978-3-030-63625-8_22.

Nogué, S., de Nascimento, L., Fernández-Palacios, J.M., Whittaker, R.J., Willis, K.J., 2013. The ancient forests of La Gomera, Canary Islands, and their sensitivity to environmental change. J. Ecol. 101 (2), 368–377. https://doi.org/10.1111/1365-2745.12051.

Nogué, S., de Nascimento, L., Froyd, C.A., Wilmshurst, J.M., de Boer, E.J., Coffey, E.E.D., Whittaker, R.J., Fernández-Palacios, J.M., Willis, K.J., 2017. Island biodiversity conservation needs paleoecology. Nat. Ecol. Evol. 1 (7), 181. https://doi.org/10.1038/s41559-017-0181.

Nogué, S., Santos, A.M., Birks, H.J.B., Björck, S., Castilla-Beltrán, A., Connor, S., Steinbauer, M.J., 2021. The human dimension of biodiversity changes on islands. Science 372 (6541), 488–491. https://doi.org/10.1126/science.abd6706.

Nogué, S., de Nascimento, L., Gosling, W.D., Loughlin, N.J.D., Montoya, E., Wilmshurst, J.M., 2022. Multiple baselines for restoration ecology. Past Global Changes Magazine 30 (1), 4–5. https://doi.org/10.22498/pages.30.1.4.

Nogué, S., Castilla-Beltrán, A., de Nascimento, L., Fernández-Palacios, E., Strandberg, N. A., Wilmshurst, J.M., Fernández-Palacios, J.M., 2024. Human impacts on islands. In: Encyclopedia of Biodiversity, pp. 567–578. https://doi.org/10.1016/B978-0-12-822562-2.00062-1.

Norder, S.J., Proios, K., Whittaker, R.J., Alonso, M.R., Borges, P.A.V., Borregaard, M.K., Cowie, R.H., Florens, F.B.V., de Frias Martins, A.M., Ibáñez, M., Kissling, W.D., de Nascimento, L., Otto, R., Parent, C.E., Rigal, F., Warren, B.H., Fernández-Palacios, J. M., van Loon, E.E., Triantis, K.A., Rijsdijk, K.F., 2019. Beyond the Last Glacial Maximum: island endemism is best explained by long-lasting archipelago configurations. Global Ecol. Biogeogr. 28 (2), 184–197. https://doi.org/10.1111/geb.12835.

Olano, J.M., Brito, P., González-Rodríguez, Á.M., Martín-Esquivel, J.L., García-Hidalgo, M., Rozas, V., 2017. Thirsty peaks: drought events drive keystone shrub decline in an oceanic island mountain. Biol. Conserv. 215, 99–106. https://doi.org/10.1016/j.biocon.2017.09.008.

Ortiz, J.E., Torres, T., Yanes, Y., Castillo, C., De La Nuez, J., Ibáñez, M., Alonso, M.R., 2005. Climatic cycles inferred from the aminostratigraphy and aminochronology of Quaternary dunes and palaeosols from the eastern islands of the Canary Archipelago. J. Quat. Sci. 21, 287–306. https://doi.org/10.1002/jqs.952.

Otto, R., García-del-Rey, E., Muñoz, P.G., Fernández-Palacios, J.M., 2010. The effect of fire severity on first-year seedling establishment in a *Pinus canariensis* forest on Tenerife, Canary Islands. Eur. J. For. Res. 129, 499–508. https://doi.org/10.1007/s10342-009-0347-6.

Pausas, J.G., 2012. Incendios Forestales. Los libros de la Catarata, Madrid, Spain.

Pérez-Angel, L.C., Sepúlveda, J., Molnar, P., Montes, C., Rajagopalan, B., Snell, K., Gonzalez-Arango, C., Dildar, N., 2020. Soil and air temperature calibrations using branched GDGTs for the Tropical Andes of Colombia: toward a pan-tropical calibration. G-cubed 21 (8). https://doi.org/10.1029/2020GC008941.

Perry, G.L., Wilmshurst, J.M., McGlone, M.S., 2014. Ecology and long-term history of fire in New Zealand. N. Z. J. Ecol. 157–176.

Peterse, F., van der Meer, J., Schouten, S., Weijers, J.W.H., Fierer, N., Jackson, R.B., Kim, J.-H., Sinninghe Damsté, J.S., 2012. Revised calibration of the MBT–CBT paleotemperature proxy based on branched tetraether membrane lipids in surface soils. Geochem. Cosmochim. Acta 96, 215–229. https://doi.org/10.1016/j.gca.2012.08.011.

Petit-Maire, N., Delibrias, G., Meco, J., Pomel, R.S., Rosso, J.C., 1987. Paleoclimats de L'île de Fuerteventura (Archipel Canarien). In: van Zinderen Bakker, E.M., Heine, K. (Eds.), Palaeoecology of Africa and the Surrounding Islands, vol. 18. A.A. Balkema, London, United Kingdom, pp. 351–356.

Prell, W.L., Kutzbach, J.E., 1987. Monsoon variability over the past 150,000 years. J. Geophys. Res. Atmos. 92 (D7), 8411–8425. https://doi.org/10.1029/JD092iD07p08411.

Raberg, J.H., Miller, G.H., Geirsdóttir, Á., Sepúlveda, J., 2022. Near-universal trends in brGDGT lipid distributions in nature. Sci. Adv. 8 (20), eabm7625. https://doi.org/10.1126/sciadv.abm7625.

Ravazzi, C., Mariani, M., Criado, C., Garozzo, L., Naranjo-Cigala, A., Perez-Torrado, F.J., Pini, R., Rodriguez-Gonzalez, A., Nogué, S., Whittaker, R.J., Fernández-Palacios, J. M., de Nascimento, L., 2021. The influence of natural fire and cultural practices on island ecosystems: insights from a 4,800-year record from Gran Canaria, Canary Islands. J. Biogeogr. 48 (2), 276–290. https://doi.org/10.1111/jbi.13995.

Reimer, P.J., Austin, W.E.N., Bard, E., Bayliss, A., Blackwell, P.G., Bronk Ramsey, C., Butzin, M., Cheng, H., Edwards, R.L., Friedrich, M., Grootes, P.M., Guilderson, T.P., Hajdas, I., Heaton, T.J., Hogg, A.G., Hughen, K.A., Kromer, B., Manning, S.W., Muscheler, R., Palmer, J.G., Pearson, C., van der Plicht, J., Reimer, R.W., Richards, D.A., Scott, E.M., Southon, J.R., Turney, C.S.M., Wacker, L., Adolphi, F., Büntgen, U., Capano, M., Fahrni, S.M., Fogtmann-Schulz, A., Friedrich, R., Köhler, P., Kudsk, S., Miyake, F., Olsen, J., Reinig, F., Sakamoto, M., Sookdeo, A., Talamo, S., 2020. The IntCal20 Northern Hemisphere radiocarbon age calibration curve (0–55 cal kBP). Radiocarbon 62 (4), 725–757. https://doi.org/10.1017/RDC.2020.41.

Richter, N., Russell, J.M., Amaral-Zettler, L., DeGroff, W., Raposeiro, P.M., Gonçalves, V., de Boer, E.J., Pla-Rabes, S., Hernández, A., Benavente, M., Ritter, C., Sáez, A., Bao, R., Trigo, R.M., Prego, R., Giralt, S., 2022. Long-term hydroclimate variability in the sub-tropical North Atlantic and anthropogenic impacts on lake ecosystems: a case study from Flores Island, the Azores. Quat. Sci. Rev. 285, 107525. https://doi.org/10.1016/j.quascirev.2022.107525.

Roberts, N., 2009. Holocene climates. In: Gornitz, V. (Ed.), Encyclopedia of Paleoclimatology and Ancient Environments. Springer, Dordrecht, The Netherlands, pp. 495–498. https://doi.org/10.1007/978-1-4020-4411-3_106.

Rodríguez González, A., 2009. *Holocene volcanism of Gran Canaria: Application of a Geographic Information System* [Doctoral Dissertation. University of Las Palmas de Gran Canaria. http://hdl.handle.net/10553/1894.

Russell, J.M., Hopmans, E.C., Loomis, S.E., Liang, J., Sinninghe Damsté, J.S., 2018. Distributions of 5- and 6-methyl branched glycerol dialkyl glycerol tetraethers (brGDGTs) in East African lake sediment: effects of temperature, pH, and new lacustrine paleotemperature calibrations. Org. Geochem. 117, 56–69. https://doi.org/10.1016/j.orggeochem.2017.12.003.

Salas, M., del Arco, M.J., Pérez de Paz, P.L., 1998. Contribución al estudio fitosociológico del pinar grancanario (Islas Canarias). Lazaroa 19, 99–117.

Santana, J., del Pino, M., Morales, J., Fregel, R., Hagenblad, J., Morquecho, A., Brito-Mayor, A., Henríquez, P., Jiménez, J., Serrano, J.G., Sánchez-Cañadillas, E., Ordóñez, A.C., Gilson, S.-P., 2024. The chronology of the human colonisation of the Canary Islands. Proc. Natl. Acad. Sci. 121 (28), e2302924121. https://doi.org/10.1073/pnas.230292412.

Schouten, S., Hopmans, E.C., Pancost, R.D., Sinninghe Damsté, J.S., 2000. Widespread occurrence of structurally diverse tetraether membrane lipids: evidence for the ubiquitous presence of low-temperature relatives of hyperthermophiles. Proc. Natl. Acad. Sci 97 (26), 14421–14426. https://doi.org/10.1073/pnas.97.26.14421.

Schouten, S., Hopmans, E.C., Sinninghe Damsté, J.S., 2013. The organic geochemistry of glycerol dialkyl glycerol tetraether lipids: a review. Org. Geochem. 54, 19–61. https://doi.org/10.1016/j.orggeochem.2012.09.006.

Schmincke, H., Sumita, M., 2012. Geological evolution of the Canary Islands. Koblenz, Germany: Görres-Druckerei und Verlag.

Sinninghe Damsté, J.S., Rijpstra, W.I.C., Hopmans, E.C., Weijers, J.W.H., Foesel, B.U., Overmann, J., Dedysh, S.N., 2011. 13,16-dimethyl octacosanedioic acid (*iso*-diabolic acid), a common membrane-spanning lipid of Acidobacteria subdivisions 1 and 3. Appl. Environ. Microbiol. 77 (12), 4147–4154. https://doi.org/10.1128/AEM.00466-11.

Sinninghe Damsté, J.S., Rijpstra, W.I.C., Hopmans, E.C., Foesel, B.U., Wüst, P.K., Overmann, J., Tank, M., Bryant, D.A., Dunfield, P.F., Houghton, K., Stott, M.B., 2014. Ether- and ester-bound *iso*-diabolic acid and other lipids in members of Acidobacteria subdivision 4. Appl. Environ. Microbiol. 80 (17), 5207–5218. https://doi.org/10.1128/AEM.01066-14.

Sinninghe Damsté, J.S., Hopmans, E.C., Pancost, R.D., Schouten, S., Geenevasen, J.A., 2000. Newly discovered non-isoprenoid glycerol dialkyl glycerol tetraether lipids in sediments. Chemical Communications 17, 1683–1684.

Sinninghe Damsté, J.S., Rijpstra, W.I.C., Foesel, B.U., Huber, K.J., Overmann, J., Nakagawa, S., Kim, J.J., Dunfield, P.F., Dedysh, S.N., Villanueva, L., 2018. An overview of the occurrence of ether- and ester-linked *iso*-diabolic acid membrane lipids in microbial cultures of the Acidobacteria: implications for brGDGT paleoproxies for temperature and pH. Org. Geochem. 124, 63–76. https://doi.org/10.1016/j.orggeochem.2018.07.006.

Smerdon, J.E., Pollack, H.N., Cermak, V., Enz, J.W., Kresl, M., Safanda, J., Wehmiller, J. F., 2004. Air-ground temperature coupling and subsurface propagation of annual temperature signals. J. Geophys. Res. Atmos. 109 (D21), D21107. https://doi.org/10.1029/2004JD005056.

Sperling, F.N., Washington, R., Whittaker, R.J., 2004. Future climate change of the subtropical North Atlantic: implications for the cloud forests of Tenerife. Clim. Change 65 (1–2), 103–123. https://doi.org/10.1023/B:CLIM.0000037488.33377.bf.

Suc, J.P., 1984. Origin and evolution of the Mediterranean vegetation and climate in Europe. Nature 307 (5947), 429–432. https://doi.org/10.1038/307429a0.

Tierney, J.E., Pausata, F.S.R., deMenocal, P.B., 2017. Rainfall regimes of the green Sahara. Sci. Adv. 3 (1), e1601503. https://doi.org/10.1126/sciadv.1601503.

Tierney, J.E., Zhu, J., King, J., Malevich, S.B., Hakim, G.J., Poulsen, C.J., 2020. Glacial cooling and climate sensitivity revisited. Nature 584 (7822), 569–573. https://doi.org/10.1038/s41586-020-2617-x.

Vannière, B., Colombaroli, D., Chapron, E., Leroux, A., Tinner, W., Magny, M., 2008. Climate versus human-driven fire regimes in Mediterranean landscapes: the Holocene record of Lago dell'Accesa (Tuscany, Italy). Quat. Sci. Rev. 27 (11–12), 1181–1196. https://doi.org/10.1016/j.quascirev.2008.02.011.

von Suchodoletz, H., Oberhänsli, H., Hambach, U., Zöller, L., Fuchs, M., Faust, D., 2010. Soil moisture fluctuations recorded in Saharan dust deposits on Lanzarote (Canary

Islands) over the last 180 ka. Quat. Sci. Rev. 29 (17–18), 2173–2184. https://doi.org/10.1016/j.quascirev.2010.05.014.
Wang, H., Liu, W., Lu, H., 2016. Appraisal of branched glycerol dialkyl glycerol tetraether-based indices for North China. Org. Geochem. 98, 118–130. https://doi.org/10.1016/j.orggeochem.2016.05.013.
Wang, H., An, Z., Lu, H., Zhao, Z., Liu, W., 2020. Calibrating bacterial tetraether distributions towards in situ soil temperature and application to a loess-paleosol sequence. Quat. Sci. Rev. 231, 106172. https://doi.org/10.1016/j.quascirev.2020.106172.
Watrin, J., Lézine, A.M., Hély, C., 2009. Plant migration and plant communities at the time of the "green Sahara". C. R. Geosci. 341 (8–9), 656–670. https://doi.org/10.1016/j.crte.2009.06.007.
Weigelt, P., Jetz, W., Kreft, H., 2013. Bioclimatic and physical characterization of the world's islands. Proc. Natl. Acad. Sci. U.S.A. 110 (38), 15307–15312. https://doi.org/10.1073/pnas.1306309110.
Weigelt, P., Steinbauer, M.J., Cabral, J.S., Kreft, H., 2016. Late Quaternary climate change shapes island biodiversity. Nature 532 (7597), 99–102. https://doi.org/10.1038/nature17443.
Weijers, J.W.H., Schouten, S., Hopmans, E.C., Geenevasen, J.A.J., David, O.R.P., Coleman, J.M., Pancost, R.D., Sinninghe Damsté, J.S., 2006. Membrane lipids of mesophilic anaerobic bacteria thriving in peats have typical archaeal traits. Environ. Microbiol. 8 (4), 648–657. https://doi.org/10.1111/j.1462-2920.2005.00941.x.
Weijers, J.W.H., Schouten, S., van den Donker, J.C., Hopmans, E.C., Sinninghe Damsté, J.S., 2007. Environmental controls on bacterial tetraether membrane lipid distribution in soils. Geochem. Cosmochim. Acta 71, 703–713. https://doi.org/10.1016/j.gca.2006.10.003.
Weijers, J.W.H., Panoto, E., van Bleijswijk, J., Schouten, S., Rijpstra, W.I.C., Balk, M., Stams, A.J.M., Sinninghe Damsté, J.S., 2009. Constraints on the biological source(s) of the orphan branched tetraether membrane lipids. Geomicrobiol. J. 26 (6), 402–414. https://doi.org/10.1080/01490450902937293.
Whittaker, R.J., Fernández-Palacios, J.M., Matthews, T.J., 2023. Island biogeography: Geo-environmental dynamics, ecology, evolution, human impact, and conservation. Oxford University Press, Oxford, United Kingdom.
Whittaker, R.J., Fernández-Palacios, J.M., 2007. Island Biogeography: Ecology, Evolution, and Conservation. Oxford University Press, Oxford.
Williams, R.H., McGee, D., Kinsley, C.W., Ridley, D.A., Hu, S., Fedorov, A., Tal, I., Murray, R.W., deMenocal, P.B., 2016. Glacial to Holocene changes in trans-Atlantic Saharan dust transport and dust-climate feedbacks. Sci. Adv. 2 (11), e1600445. https://doi.org/10.1126/sciadv.1600445.
Willis, K.J., Birks, H.J., 2006. What is natural? The need for a long-term perspective in biodiversity conservation. Science 314 (5803), 1261–1265. https://doi.org/10.1126/science.1122667.
Yanes, Y., 2008. Palaeoclimate of the last 50.000 years in the Canary Islands inferred from the stable isotopes composition of the land snail shells. In: Joint Meeting of the Geological Society of America, Soil Science Society of America, American Society of Agronomy, and the Crop Science Society of America, Gulf Coast Association of Geological Societies, and the Gulf Coast Section of SEPM.
Yanes, Y., Yapp, C.J., Ibáñez, M., Alonso, M.R., De-la-Nuez, J., Quesada, M.L., Castillo, C., Delgado, A., 2011. Pleistocene–Holocene environmental change in the Canary Archipelago as inferred from the stable isotope composition of land snail shells. Quat. Res. 75 (3), 658–669. https://doi.org/10.1016/j.yqres.2010.11.004.
Zühlsdorff, C., Wien, K., Stuut, J.-B.W., Henrich, R., 2007. Late Quaternary sedimentation within a submarine channel–levee system offshore Cap Timiris, Mauritania. Mar. Geol. 240 (1–4), 217–234. https://doi.org/10.1016/j.margeo.2007.02.005.
Zhao, M., Beveridge, N.A.S., Shackleton, N.J., Sarnthein, M., Eglinton, G., 1995. Molecular stratigraphy of cores off northwest Africa: Sea surface temperature history over the last 80 ka. Paleoceanography 10 (3), 661–675. https://doi.org/10.1029/94PA03354.
Zühlsdorff, C., Hanebuth, T.J.J., Henrich, R., 2008. Persistent quasi-periodic turbidite activity off Saharan Africa and its comparability to orbital and climate cyclicities. Geo Mar. Lett. 28, 87–95. https://doi.org/10.1007/s00367-007-0092-0.